

Visco-plastic fluid displacements in near-vertical narrow eccentric annuli: prediction of travelling-wave solutions and interfacial instability

By S. PELIPENKO¹ AND I. A. FRIGAARD^{2,3†}

¹54 St Peter's Street, London N1 8JT, UK

²Department of Mathematics, University of British Columbia, 1984 Mathematics Road, Vancouver, BC, V6T 1Z2, Canada

³Department of Mechanical Engineering, University of British Columbia, 2324 Main Mall, Vancouver, BC, V6T 1Z4, Canada

(Received 19 September 2003 and in revised form 5 August 2004)

We present new results on the laminar displacement of Herschel–Bulkley fluids along narrow eccentric annuli. We adopt a Hele–Shaw modelling approach and consider the possibility that a long displacement finger should advance along the wide side of the annulus. We deduce conditions under which this cannot happen. We also analyse local instability of the interface on wide and narrow sides of the annulus using the Muskat approach. We thus show that it is possible to have both steady and unsteady travelling-wave solutions, for which the interface is locally stable.

We show how steady stable displacements arise from an increase in effective viscosity difference between displacing and displaced fluids and also analyse effects of buoyancy on the displacement. As opposed to many studies of Hele–Shaw displacements, the principle focus is on identifying stable steady displacements. Finally, we show how predictions of our model, derived from the Navier–Stokes equations using well-defined scaling arguments, compare with some of the *ad hoc* rule-based design systems that are currently used in the oil industry for design of primary cementing displacements.

1. Introduction

The aim of this paper is to derive conditions for stable/unstable and steady/unsteady displacements of Herschel–Bulkley fluids along a narrow eccentric annulus. The motivation for the study comes from the industrial process of primary cementing. This process involves the displacement of one non-Newtonian fluid by another, pumped axially along the annulus at a constant imposed flow rate, see figure 1. The flows that we consider are laminar and the annuli considered have annular gaps that are narrow with respect to both circumferential and axial length scales. Thus, a Hele–Shaw modelling approach is appropriate and in this paper we adopt a two-dimensional model derived by Bittleston, Ferguson & Frigaard (2002); see also Pelipenko & Frigaard (2004*a, b*), that we outline in §2 below. Those unfamiliar with this process may consult Nelson (1990) or the above papers for further references.

† Author to whom correspondence should be addressed.

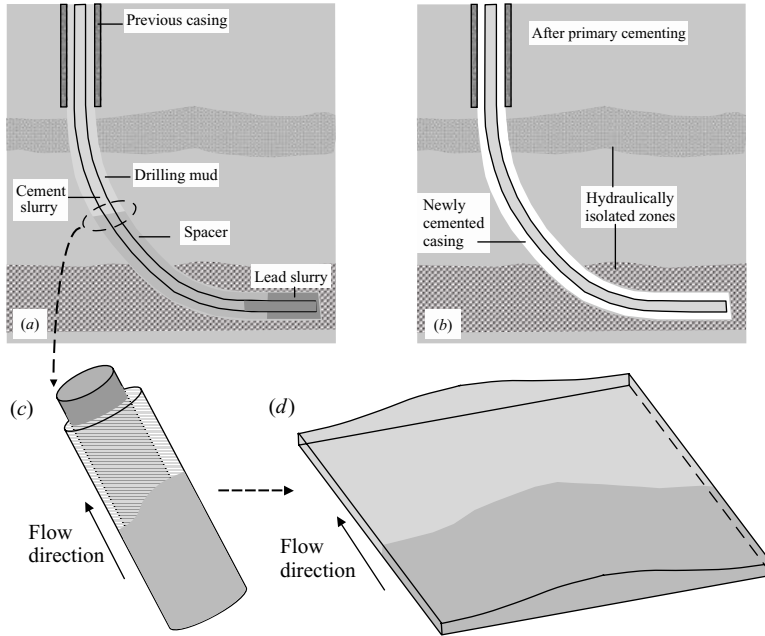


FIGURE 1. Schematic of the primary cementing process: (a) during the cementing of a new casing; (b) after cementing a new casing; (c) the narrow eccentric annular displacement flow; (d) unwrapping of the annulus into a Hele-Shaw displacement cell.

From the industrial perspective, a good displacement corresponds to displacement of the *in situ* fluid perfectly, all around that annulus, with little instability/mixing at the interface and with the interface moving steadily at the mean pumping speed. We shall seek to define the parameters for which such stable steady/travelling-wave displacements occur. In practice, this means identifying conditions where either unsteadiness or instability occur. First, we clarify these terms.

Local stability/instability: Consider a vertical narrow concentric annulus along which fluid 1 displaces fluid 2 at steady speed. Taking a Hele-Shaw approach, it is evident that there exists a planar displacement front solution, moving vertically upwards at the mean pumping speed. Apart from periodicity in the azimuthal direction, the equations are identical with any planar Hele-Shaw displacement. For certain combinations of viscosity (rheology) and density we expect there to be a critical velocity determining the onset of viscous fingering, i.e. this is purely a non-Newtonian Saffman–Taylor fingering paradigm. It is this phenomenon that we use to classify the interface as locally unstable/stable.

Steady/unsteady displacement fronts: Consider a single fluid flowing axially in a narrow eccentric annulus. It is evident that the fluid moves faster on the wide side of the annulus than the narrow side (see e.g. Walton & Bittleston 1991; Szabo & Hassager 1992). If we instantaneously colour the fluid red and blue, respectively, above and below a certain axial position, we will see the interface between red and blue fluid elongate on the wide side of the annulus, where the velocity is largest. This is a dispersion phenomenon, and is primarily due to eccentricity. By varying the rheology and/or density of only the (blue) displacing fluid 1, we might hope to reduce the dispersion effect and perhaps even eliminate it. Although we cannot expect that the

interface will be planar, it may advance at the mean pumping speed all around the annulus, i.e. a steady-state/travelling-wave solution.

We will consider how to predict the above two phenomena. We acknowledge that the distinction between steady/unsteady and locally stable/unstable can become blurred. For example, the transition from steady to unsteady displacement front can also be considered as a form of instability, albeit non-local (see Pelipenko & Frigaard 2004*b*). There are also other instabilities of a local nature that might arise in a displacement flow, e.g. interfacial shear instabilities. These we have not yet studied in detail. Thus our study, as any on such a complex system, will be incomplete.

1.1. Related literature

It is clear that there will be some relation between our analysis and studies of Hele-Shaw and porous media displacements. This is, however, a vast area and it is not sensible to attempt a review here.† We remark that the main thrust of research in Hele-Shaw and Saffman–Taylor type displacements has been to study and characterize instability, whereas the (industrial) objectives are to arrive at a stable steady displacement. Apart from geometrical complications, a second difference is in the fluids that we consider are non-Newtonian: inelastic shear-thinning fluids with a yield stress, for which there is significantly less literature.

In relation to modelling the flow of yield stress fluids in Hele-Shaw cells and porous media, respectively, we refer to Coussot (1999) and to Barenblatt, Entov & Ryzhik (1990). In the porous media case, these flows are often characterized by a limiting pressure gradient. There have been some studies of viscous fingering in such fluids. Pascal has studied extensively the classical planar interfacial instabilities in porous media displacements (Pascal 1984*a, b*, 1986), i.e. planar and radial displacement fronts. Approximate criteria for fingering in a planar Hele-Shaw displacement have been developed by Coussot (1999), Lindner (2000), Lindner, Coussot and Bonn (2000). Alexandrou & Entov (1997) have studied motion of a two-dimensional bubble propagating in a Hele-Shaw cell. Viscous fingering in annular geometries is neither studied nor understood.

Q1

With regard to the phenomenon of steady/unsteady non-Newtonian displacements in an eccentric annulus, there appears to be very little study other than that related to our own work in Bittleston *et al.* (2002) and Pelipenko & Frigaard (2004*a, b*). The focus of Bittleston *et al.* (2002) is a detailed exposition of the derivation of a comprehensive model to simulate the primary cementing displacement process in two dimensions; multiple fluids, fluctuating flow rates, slow axial variations in annular radii, eccentricity and deviation are all accounted for. The results presented in Bittleston *et al.* (2002) mostly constitute example displacement simulations for industrially relevant parameters, but there is no analysis of the actual displacement process.

In a Newtonian Hele-Shaw displacement, the field equations for either stream function or pressure are linear. Here, they are nonlinear and are expressed (rigorously) as a variational inequality. In Pelipenko & Frigaard (2004*a*), we show that for practical interface configurations, physically sensible fluid properties and well geometries, there exists a unique (weak) solution for the stream function Ψ . Also in Pelipenko & Frigaard (2004*a*) we show that, for certain fluid properties, it is possible to find steady-state (travelling-wave) solutions, i.e. an interface that advances steadily along the annulus at the mean pumping speed. These solutions can be found for concentric

† A bibliography of over 500 papers, books and articles can be found at: <http://www.maths.ox.ac.uk/~howison/Hele-Shaw/>.

annuli and, via a perturbation method, for slightly eccentric annuli. We do not consider stability of these steady-state displacement fronts, as we do here.

In Pelipenko & Frigaard (2004b), first we have considered how to solve the variational inequality for Ψ accurately in two dimensions using the augmented Lagrangian approach. The advantage of this method is that unyielded regions of the flow are accurately represented. This is important since such regions represent a significant and detrimental process feature in which the fluid does not move, i.e. typically where drilling mud is not removed from the narrow side of the annulus. Also in Pelipenko & Frigaard (2004b), we use our two-dimensional computational method to investigate (global) stability of the steady-state displacement profiles that we found in Pelipenko & Frigaard (2004a), i.e. the transition from steady to unsteady as the eccentricity is increased. We show that steady-state stability and loss of stability is a global phenomenon, i.e. depends on the flow field in a non-local way. Although our work in Pelipenko & Frigaard (2004b) leads to a detailed understanding of the flow field close to a stable steady state and how the interface converges to the steady state, the method is not ideal for large-scale parametric study of stability. One problem is that using two-dimensional computations is time consuming. A second problem is that as marginal stability is approached in the parameter space, it takes an infinite time for a transient interface to converge to a stable steady state. Thus, simulation methods necessarily become ineffective.

1.2. Outline of the paper

A brief outline of the paper is as follows. In §2, we outline a simplified version of the Hele-Shaw displacement model from Bittleston *et al.* (2002), which is the starting point for all the analysis in the paper. Section 3 explains the methods used for classifying displacement as steady/unsteady and (locally) stable/unstable. In §4, we present analytical results, derived using perturbation methods for annuli of small eccentricity. Sections 5 and 6 look at how the dispersive effects of eccentricity can be countered by rheology and density differences. In §7, we show that our predictions of steady/unsteady displacements compare very favourably with a typical industrial rule-based design system. The paper ends with a summary of results in §8.

2. Hele-Shaw modelling of cementing displacements

We consider a simplified version of the model developed by Bittleston *et al.* (2002). The simplification that we make is that the annulus is locally uniform in the axial direction, i.e. over a length scale that is long in comparison to the azimuthal scale. This is justified for the slowly varying geometries of typical wells and is also relevant to laboratory-scale experiments. Consider therefore a uniform section of annulus with axis at fixed angle of inclination, β , to the vertical, see figure 2. The model in Bittleston *et al.* (2002); Pelipenko & Frigaard (2004a) consists of averaging across the narrow annular gap to eliminate radial variations, thus effectively unwrapping the annulus into a Hele-Shaw cell (figure 1d).

Dimensionless spatial coordinates are $(\phi, \xi) \in (0, 1) \times (0, Z)$. Here, ϕ is the azimuthal coordinate with $\phi=0$ denoting the wide side of the annulus and $\phi=1$ the narrow (lower) side. The flow is assumed symmetric about $\phi=0$, and thus only half the annulus is considered. This assumption implies that the narrow side of the annulus is always lying on the lower side of the well. The ξ -coordinate measures axial depth upwards along the annulus (see figure 2). Here, Z denotes the length of the section of well to be cemented and $Z \gg 1$ since the length scale used for scaling the

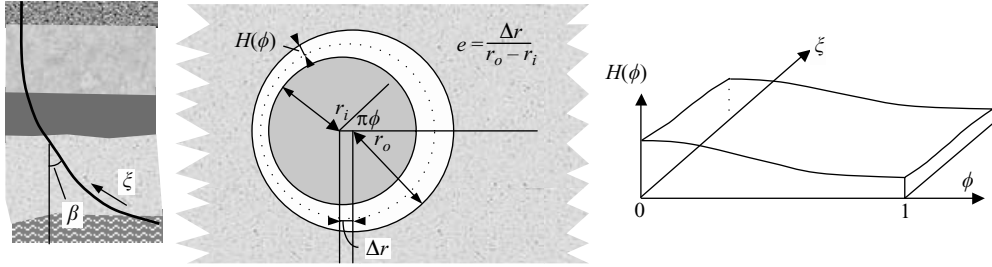


FIGURE 2. Geometry of the narrow eccentric annulus, mapped to the Hele-Shaw cell geometry.

equations is half of the mean circumference, (typically ≈ 0.5 m), and typical lengths of cemented sections are of the order of hundreds of metres. The half-gap width H varies only with ϕ ; $H(\phi)$ is defined by:

$$H(\phi) = 1 + e \cos \pi \phi, \quad (2.1)$$

which is a narrow-gap approximation. Here, $e \in [0, 1)$ is the annulus eccentricity (see figure 2); $e=0$ corresponds to a concentric annulus, $e=1$ implies contact between casing and outer wall, on the narrow side of the annulus.

The annulus is initially full of fluid 2, which is displaced by fluid 1. The displacement model is most easily understood via a fluid concentration formulation, although for the analysis later in this paper we shall adopt an interface tracking formulation, see §2.2. We consider only two fluids and denote by \bar{c} the concentration of fluid 1, which satisfies the advection equation:

$$\frac{\partial}{\partial t} [H\bar{c}] + \frac{\partial}{\partial \phi} [H\bar{v}\bar{c}] + \frac{\partial}{\partial \xi} [H\bar{w}\bar{c}] = 0. \quad (2.2)$$

The averaged velocity components in the (ϕ, ξ) -directions are (\bar{v}, \bar{w}) . The fluids are considered incompressible and (\bar{v}, \bar{w}) are described by means of a stream function Ψ :

$$\frac{\partial \Psi}{\partial \phi} = H\bar{w}, \quad \frac{\partial \Psi}{\partial \xi} = -H\bar{v}. \quad (2.3)$$

The stream function is found from the following field equation:

$$\nabla \cdot \mathbf{S} = -f. \quad (2.4)$$

The term f , defined below, contains density gradient terms. The left-hand side of (2.4) is elliptic and, in the case of two Newtonian fluids, would simplify to:

$$\mathbf{S} = \frac{3\kappa(\bar{c})}{H^3} \nabla \Psi, \quad \nabla \cdot \left[\frac{3\kappa(\bar{c})}{H^3} \nabla \Psi \right] = -f, \quad (2.5)$$

which should be familiar from Hele-Shaw modelling (note that here we work with the stream function formulation, rather than the usual pressure formulation, see §2.1).

For the situations we consider, the underlying fluids are modelled as Herschel–Bulkley fluids: $m=1/n$ is the inverse power law index, τ_Y is the yield stress and κ is the consistency (for a Newtonian fluid $m=1$ and $\tau_Y=0$). We assume that the fluids are shear-thinning throughout ($m \geq 1$), since this is usual with oilfield fluids. For these fluids, the equivalent relation to the first part of (2.5) is given in

Bittleston *et al.* (2002):

$$\mathbf{S} = \left[\frac{\chi(|\nabla\Psi|) + \tau_Y/H}{|\nabla\Psi|} \right] \nabla\Psi \iff |\mathbf{S}| > \frac{\tau_Y}{H}, \quad (2.6)$$

$$|\nabla\Psi| = 0 \iff |\mathbf{S}| \leq \frac{\tau_Y}{H}. \quad (2.7)$$

This is essentially a constitutive relationship. The vector field \mathbf{S} represents the modified pressure gradient field (see §2.1 for a precise definition). We note that $|\mathbf{S}| = (\chi + \tau_Y/H)$, which corresponds dimensionlessly, to the absolute value of the modified pressure gradient required to push an areal flow rate $|\nabla\Psi|$ through a plane channel of half-width H . The function $\chi = \chi(|\nabla\Psi|; H, \tau_Y, \kappa, m)$ is defined implicitly from the relation:

$$|\nabla\Psi| = \begin{cases} 0, & \chi \leq 0, \\ \frac{H^{m+2}}{\kappa^m(m+2)} \frac{\chi^{m+1}}{(\chi + \tau_Y/H)^2} \left[\chi + \frac{(m+2)\tau_Y}{(m+1)H} \right], & \chi > 0. \end{cases} \quad (2.8)$$

Underlying (2.8) is a model of the flow of a Herschel–Bulkley fluid along a plane channel in the direction of the modified pressure gradient. Thus, if $|\mathbf{S}| \leq \tau_Y/H$ then $|\nabla\Psi| = 0$, and there is no fluid flow. Physically, the pressure gradient is not strong enough to overcome the yield stress in that section of the annulus. At such points, \mathbf{S} is bounded, but is indeterminate. At points where $|\nabla\Psi| > 0$, the fluid is flowing. All buoyancy terms have been collected on the right-hand side of (2.4) in the term f :

$$f = \nabla \cdot \left(\frac{\rho(\bar{c}) \cos \beta}{St^*}, \frac{\rho(\bar{c}) \sin \beta \sin \pi\phi}{St^*} \right) = \nabla \cdot \tilde{\mathbf{f}}, \quad (2.9)$$

where St^* is the global Stokes number for the flow (typically $St^* < 1$), defined by:

$$St^* = \frac{\hat{\mu}^* \hat{w}^*}{\hat{\rho}^* \hat{g} (\hat{d}^*)^2}.$$

To recover dimensional quantities: axial and azimuthal velocities have been scaled with the mean flow velocity, \hat{w}^* , lengths with the half-circumference, $\pi \hat{r}_a^*$ (here, \hat{r}_a^* is the mean radius). A rate of strain scale is obtained by dividing \hat{w}^* by the half-gap width, $\hat{d}^* = (\hat{r}_o - \hat{r}_i)/2$, and this is used with the constitutive laws to derive a viscosity scale, $\hat{\mu}^*$. The pressure gradient balances with the leading-order shear-stress scale, as always in a Hele-Shaw flow. Finally, $\hat{\rho}^*$ is the density scale and \hat{g} the acceleration due to gravity.

Boundary conditions for (2.2) are symmetry of concentration at $\phi = 0, 1$, and specification of any inflowing fluid concentrations at the ends, $\xi = 0, Z$, i.e. $\bar{c} = 0$ or $\bar{c} = 1$, accordingly. For the stream-function equation (2.4), boundary conditions are

$$\Psi(0, \xi, t) = 0, \quad \Psi(1, \xi, t) = 1, \quad (2.10)$$

$$\frac{\partial \Psi}{\partial \xi}(\phi, Z, t) = 0, \quad \frac{\partial \Psi}{\partial \xi}(\phi, 0, t) = 0. \quad (2.11)$$

2.1. Pressure formulation

More commonly, a Hele-Shaw model is formulated in terms of the pressure field and this is also possible here. The components of $\mathbf{S} = (S_\phi, S_\xi)$ have the alternate representation:

$$S_\phi = -\frac{\partial p}{\partial \xi} - \frac{\rho(\bar{c}) \cos \beta}{St^*}, \quad S_\xi = \frac{\partial p}{\partial \phi} - \frac{\rho(\bar{c}) \sin \beta \sin \pi\phi}{St^*}, \quad (2.12)$$

from which it is possible to eliminate the stream function and derive a pressure equation in place of (2.4). However, the pressure will be indeterminate in regions where $|S| \leq \tau_y/H$, and for this reason the stream-function formulation is preferable. We note that this is also the case in porous media flows with a limiting pressure gradient, which are mathematically similar (see e.g. Barenblatt *et al.* 1990; Goldstein & Entov 1989).

2.2. Interface tracking

The formulation with (2.2) requires us to interpret the interface as a level line of the concentration field, e.g. $\bar{c}(\phi, \xi, t) = 0.5$, and also to specify closure laws for the mixture fluid properties, i.e. as functions of \bar{c} . In Pelipenko & Frigaard (2004a), we have also derived an alternative formulation that tracks the interface using a kinematic equation, as opposed to solving (2.2) for the concentration. The domain is divided into two fluid domains: Ω_1 for the displacing (lower) fluid 1, and Ω_2 for the displaced (upper) fluid 2, in each of which (2.4) is replaced by:

$$\nabla \cdot \mathbf{S}_1 = 0, \quad (\phi, \xi) \in \Omega_1, \quad (2.13)$$

$$\nabla \cdot \mathbf{S}_2 = 0, \quad (\phi, \xi) \in \Omega_2, \quad (2.14)$$

with \mathbf{S}_1 and \mathbf{S}_2 defined as in (2.6)–(2.7), with properties $\rho_1, \tau_{1,Y}, \kappa_1, m_1$ in fluid 1 and $\rho_2, \tau_{2,Y}, \kappa_2, m_2$ in fluid 2. The interface is denoted by $\phi = \phi_i(\xi, t)$, and satisfies the kinematic condition:

$$\frac{\partial \phi_i}{\partial t} + \bar{w} \frac{\partial \phi_i}{\partial \xi} = \bar{v}. \quad (2.15)$$

The leading-order continuity conditions at the interface are that the stream function Ψ and the pressure p are continuous across the interface. Assuming sufficient regularity of the interface, the former condition assures that the normal velocity (i.e. the derivative of Ψ along the interface), is well defined at the interface. Differentiating the pressure along the interface, we find:

$$\left[\left(S_{k,\xi} \frac{\partial \phi_i}{\partial \xi} - S_{k,\phi} \right) + \left(\frac{\rho_k \sin \beta \sin \pi \phi}{St^*} \frac{\partial \phi_i}{\partial \xi} - \frac{\rho_k \cos \beta}{St^*} \right) \right]_1^2 = 0. \quad (2.16)$$

Equation (2.16) defines the jump in the normal derivative of Ψ across the interface. It is this formulation that we shall adopt hereinafter.

2.3. Regarding Hele-Shaw and similar modelling approaches for yield stress fluids

Above, we have used a Hele-Shaw approach, which essentially consists of averaging across the narrow annular gap. In §3, we shall use a lubrication approach in which there is a slow axial variation in the displacement front. In Bittleston *et al.* (2002), the model derived is applied to annular geometries with slow axial variation (although here we consider a uniform annular section). For each of these cases there may be a concern about the validity of lubrication/thin-film methods in our analysis.

As pointed out first by Lipscomb & Denn (1984), use of a naive regular perturbation method can fail to give the correct yield surface position in a geometry with large aspect ratio. The key problem here is that the classical scaling arguments lead to a prediction of an unyielded plug speed that has a slow extensional variation (and hence is not a true plug). There are many examples of this so-called *lubrication paradox* in the literature. A modified approach is to rescale the variables in the vicinity of the (pseudo-)yield surface, so that the shear and extensional stresses balance. This has been done, for example, in Walton & Bittleston (1991) and Balmforth & Craster (1999). The solutions obtained by Walton & Bittleston (1991) consist of two regions:

those that are truly unyielded and those that have an extensional shear (the pseudo-plug). The flow studied in Balmforth & Craster (1999) is a thinning film, for which there is only a pseudo-plug. The method is, however, similar to Walton & Bittleston (1991). Comparing the asymptotic results in Walton & Bittleston (1991) with the computations in Szabo & Hassager (1992), (which use no regularization), indicates good agreement and shows that velocity fields and true yield surface positions can be computed for certain lubrication flows using singular perturbation methods. In using these methods, the stress fields remain indeterminate within the true plug regions, as with the Bingham model, but are determinate within pseudo-plugs.

The following points should be noted, regarding the naive regular perturbation method, which underlies (2.8), and its comparison with the velocity computed via singular perturbation methods such as in Walton & Bittleston (1991) and Balmforth & Craster (1999). (i) The regular perturbation method does give an outer velocity field that is an $o(\delta)$ approximation to the true velocity field, where δ denotes the small parameter, i.e. aspect ratio. Thus, we should expect predictions of gap-averaged velocities from expressions such as (2.8) will give an $o(\delta)$ approximation to the gap-averaged velocity. (ii) One case where regular perturbation methods do not break down in thin-film/lubrication geometries is where there is zero flow, i.e. if unyielded fluid abuts a wall. In this case, the regular perturbation method predicts a zero plug velocity, which thus has no extensional strain rate. In our case, this corresponds to the case of having fluid wholly immobile on the narrow side of the annulus, i.e. static mud channels should be correctly predicted. Where our model will (implicitly) have a yield surface (although this is below the resolution of the model) is in the centre of each annular gap wherever the fluid is mobile. This is, however, irrelevant, since there is no intention of predicting a yield surface at this resolution – only the gap-averaged velocity is required.

3. Steady/unsteady and locally stable/unstable displacements

As explained in §1, we would like to determine whether a displacement front between a given pair of fluids in a given annular geometry will be steady/unsteady and locally stable/unstable. In our previous work, we have assumed that the displacements have a locally stable interface. The results in Bittleston *et al.* (2002) and Pelipenko & Frigaard (2004*a, b*) suggest that one of three situations occurs when one fluid displaces another along a uniform eccentric annulus.

(a) *Steady displacement.* Both fluids are fully yielded. The interface is stationary in a frame of reference that moves with the mean speed of the flow (travelling wave).

(b) *Unsteady displacement.* Both fluids are fully yielded and the displacing fluid moves up on the wide side of the annulus faster than on the narrow side, hence the interface elongates.

(c) *Static mud channel.* This is a subcategory of an unsteady displacement, where either the displaced fluid or both fluids can be unyielded (hence stationary) on the narrow side of the annulus. The interface between the fluids simply does not move on the narrow side, and hence elongates.

In this section we consider first how to predict steady and unsteady displacement fronts by means of a lubrication approximation (see §3.1). Secondly, we consider how to predict local instability of the interface (see §3.4).

3.1. Lubrication model derivation

As a starting point for our analysis of steady/unsteady displacements, we adopt the interface tracking formulation of §2.2. The overall idea here is to assume a highly

elongated interface that is more advanced on the wide side than on the narrow side.† Making the assumption that the streamlines are pseudo-parallel to the annulus axis we derive a lubrication-type model of the displacement. We analyse this model in order to predict the interface speed, on both wide and narrow sides of the annulus. Finally, we use the computed interface speed to classify the displacement, (a)–(c), as above. Note that this is a non-local analysis, as implied necessary by Pelipenko & Frigaard (2004b).

As with all lubrication approaches, a small parameter $\varepsilon \ll 1$ is required. Here $\varepsilon^{-1} \gg 1$, represents a length scale in the axial direction over which the streamlines, interface and modified pressure gradient field are all pseudo-parallel. This length scale is arbitrary, but must be long relative to the $O(1)$ circumferential scale. In the laboratory setting, we could relate ε^{-1} to the length of a pilot-scale annular flow loop. In an oilfield setting, we might assume that the geometry was approximately uniform over say a stand of casing (~ 10 m) and base ε^{-1} on this. Since we re-scale time as well as axial length, the exact interpretation of ε is not critical. To derive our leading-order model, we take the asymptotic limit $\varepsilon \rightarrow 0$. We make the following near-axial flow assumptions.

(i) *Streamlines are pseudo-parallel to the annulus axis*: so that the main velocity component is in the ξ -direction. Thus we have

$$\left| \frac{\partial \Psi}{\partial \xi} \right| = O(\varepsilon), \quad \left| \frac{\partial \Psi}{\partial \phi} \right| = O(1). \quad (3.1)$$

(ii) *Interface is pseudo-parallel to the annulus axis*: i.e. is highly elongated in the ξ -direction. Denoting the interface by $\phi = \phi_i(\xi, t)$ this translates into

$$\left| \frac{\partial \phi_i}{\partial \xi} \right| = O(\varepsilon). \quad (3.2)$$

(iii) *Modified pressure gradient field*. S_k has its main component in the ϕ -direction, driving the flow axially:

$$|S_{k,\xi}| = O(\varepsilon), \quad |S_{k,\phi}| = O(1). \quad (3.3)$$

Note that this follows directly from (i) and the definition of S in the case where the fluids are yielded. Otherwise, this is an additional assumption.

With the above assumptions, we re-scale axial length and time variables by:

$$z = \varepsilon \xi, \quad \tilde{t} = \varepsilon t. \quad (3.4)$$

For the velocity and pressure, we set

$$W = \bar{w}, \quad V = \varepsilon \bar{v}, \quad P = \varepsilon p, \quad (3.5)$$

and write $\Psi(\phi, z)$ for the streamfunction as before. Note that $V = -\Psi_z = O(1)$, following this re-scaling. The kinematic equation for the interface $\phi = \phi_i(z, \tilde{t})$ becomes:

$$\frac{\partial \phi_i}{\partial \tilde{t}} + W \frac{\partial \phi_i}{\partial z} = V. \quad (3.6)$$

† The reverse situation is not considered, i.e. if the interface elongates ahead of the mean pumping speed, it is always assumed to do so on the wide side. This might not always be valid, e.g. in a near-horizontal well where dense fluids can slump to the lower side.

Substituting for the streamfunction:

$$H(\phi_i) \frac{\partial \phi_i}{\partial \tilde{t}} + \frac{\partial \Psi}{\partial \phi}(\phi_i, z) \frac{\partial \phi_i}{\partial z} + \frac{\partial \Psi}{\partial z}(\phi_i, z) = 0. \quad (3.7)$$

Rewriting the first term and grouping the second and third together we have:

$$\frac{\partial}{\partial \tilde{t}} \left[\int_0^{\phi_i} H(\phi) d\phi \right] + \frac{\partial}{\partial z} [\Psi(\phi, z)|_{\phi=\phi_i(z)}] = 0. \quad (3.8)$$

The first term above is the time derivative of the *volumetric* interface position, $\Phi_i(z, \tilde{t})$:

$$\Phi_i(z, \tilde{t}) = \int_0^{\phi_i(z, \tilde{t})} H(\phi) d\phi = \phi_i(z, \tilde{t}) + \frac{e}{\pi} \sin \pi \phi_i(z, \tilde{t}), \quad (3.9)$$

i.e. $\Phi_i(z, \tilde{t})$ represents the volume fraction of fluid 1 at depth z . The relationship between ϕ_i and Φ_i is one-to-one, so we may write $\phi_i = \phi_i(\Phi_i)$. Below, we shall see that for the lubrication assumptions, the z -dependency of $\Psi(\phi, z)$ is wholly through $\phi_i(z)$, (equivalently $\Phi_i(z)$). We therefore write $\Psi(\phi, z) = \Psi(\phi, \phi_i(z))$ and introduce $q(\Phi_i)$:

$$q(\Phi_i) = \Psi(\phi, \phi_i(z))|_{\phi=\phi_i(z)} : \quad \phi_i(z) = \phi_i(\Phi_i(z)). \quad (3.10)$$

Using this notation, we obtain the following hyperbolic equation for propagation of the (volumetric) interface position, $\Phi_i(z, \tilde{t})$:

$$\frac{\partial \Phi_i}{\partial \tilde{t}} + \frac{\partial}{\partial z} q(\Phi_i) = 0. \quad (3.11)$$

It remains to find the function $q(\Phi_i)$ at each interface position.

Using the lubrication assumptions for the streamfunction Ψ and modified pressure gradient S , to leading order in each fluid k we have:

$$|\nabla \Psi| \sim \left| \frac{\partial \Psi}{\partial \phi} \right|, \quad \frac{\partial}{\partial \phi} S_{k,\phi} = 0. \quad (3.12)$$

Thus, to leading order, we expect that $S_{k,\phi}$ will be independent of ϕ in each fluid domain. By definition we have:

$$S_{k,\phi} = -\frac{\partial P}{\partial z} - \frac{\rho_k \cos \beta}{St^*}. \quad (3.13)$$

Secondly, by assumption:

$$S_{k,\xi} = S_{k,z} = \frac{1}{\varepsilon} \frac{\partial P}{\partial \phi} + \frac{\rho_k \sin \beta \sin \pi \phi}{St^*} \sim O(\varepsilon), \quad (3.14)$$

(note that $O(\varepsilon)$ above also follows from the scaling of the streamfunction gradients, in a yielded region). Thus, it follows that

$$\frac{\partial P}{\partial \phi} \sim -\varepsilon \rho_k \sin \beta \sin \pi \phi / St^* + O(\varepsilon^2),$$

to leading order, i.e. the azimuthal gradient is simply the static gradient in each fluid. Now consider (2.16), which is equivalent to continuity of the tangential derivative of the pressure along the interface. This can also be written as:

$$\left[\frac{\partial P}{\partial z} + \frac{\partial P}{\partial \phi} \frac{\partial \phi_i}{\partial z} \right]_1 = 0. \quad (3.15)$$

Thus, since $\partial P/\partial\phi = O(\varepsilon)$, to leading order this becomes

$$\left[\frac{\partial P}{\partial z}\right]_1^2 = 0, \quad (3.16)$$

i.e. the pressure is continuous at the interface and differentiable along the interface. Thus, integrating (3.14), we find:

$$P(\phi, z, \tilde{t}) = \begin{cases} P(0, z, \tilde{t}) - \varepsilon \frac{\rho_1(1 - \cos \pi\phi) \sin \beta}{\pi S t^*} + O(\varepsilon^2), & \phi \in [0, \phi_i(z, \tilde{t})], \\ P(0, z, \tilde{t}) - \varepsilon \frac{(\rho_1 - \rho_2 \cos \pi\phi - [\rho_1 - \rho_2] \cos \pi\phi_i) \sin \beta}{\pi S t^*} + O(\varepsilon^2), & \phi \in (\phi_i(z, \tilde{t}), 1]. \end{cases} \quad (3.17)$$

Thus, to $O(\varepsilon)$ we have:

$$S_{k,\phi}(z, \tilde{t}) \sim -\frac{\partial P}{\partial z}(0, z, \tilde{t}) - \frac{\rho_k \cos \beta}{S t^*},$$

or, alternatively,

$$S_{1,\phi}(z, \tilde{t}) \sim A(z, \tilde{t}), \quad S_{2,\phi}(z, \tilde{t}) \sim A(z, \tilde{t}) - b, \quad (3.18)$$

where b is a buoyancy parameter, given by:

$$b = \frac{\rho_2 - \rho_1}{S t^*} \cos \beta. \quad (3.19)$$

Note that, typically, b is negative. The function $A(z, \tilde{t})$ represents the leading-order modified pressure gradient in the axial direction, within fluid 1. In order to find the stream function at each (z, \tilde{t}) , we need only find $A(z, \tilde{t})$, which we do by using the boundary condition at $\phi = 1$, i.e.

$$1 = \Psi(1, z, \tilde{t}) = \int_0^{\phi_i} \frac{\partial \Psi}{\partial \phi} \Big|_{k=1} d\phi + \int_{\phi_i}^1 \frac{\partial \Psi}{\partial \phi} \Big|_{k=2} d\phi. \quad (3.20)$$

To evaluate the integrands, observe that to leading order in ε , we have

$$S_k \sim |S_{k,\phi}|, \quad |\nabla \Psi| \sim \left| \frac{\partial \Psi}{\partial \phi} \right|.$$

Thus, from (2.8) we find:

$$\frac{\partial \Psi}{\partial \phi} \Big|_{k=1} = \text{sgn}(A) \begin{cases} 0, & |A| \leq \tau_{1,Y}/H, \\ \frac{H^{m_1+2}}{\kappa_1^{m_1+1}(m_1+2)} \frac{(|A| - \tau_{1,Y}/H)^{m_1+1}}{|A|^2} \left[|A| + \frac{\tau_{1,Y}/H}{m_1+1} \right], & |A| > \tau_{1,Y}/H, \end{cases} \quad (3.21)$$

$$\frac{\partial \Psi}{\partial \phi} \Big|_{k=2} = \text{sgn}(A-b) \begin{cases} 0, & |A-b| \leq \tau_{2,Y}/H, \\ \frac{H^{m_2+2}}{\kappa_2^{m_2+1}(m_2+2)} \frac{(|A-b| - \tau_{2,Y}/H)^{m_2+1}}{|A-b|^2} \left[|A-b| + \frac{\tau_{2,Y}/H}{m_2+1} \right], & |A-b| > \tau_{2,Y}/H. \end{cases} \quad (3.22)$$

Equation (3.20) is a nonlinear equation for A . It is straightforward to show that the flow rate $Q(A)$:

$$Q(A) = \int_0^{\phi_i} \frac{\partial \Psi}{\partial \phi} \Big|_{k=1} d\phi + \int_{\phi_i}^1 \frac{\partial \Psi}{\partial \phi} \Big|_{k=2} d\phi$$

increases strictly monotonically[†] with A close to the solution of $Q(A) = 1$, and hence (3.20) has a unique solution $A = A(\phi_i(z, \tilde{t}))$.

Physically, (3.20) represents finding the modified pressure gradient, $A(\phi_i)$, required to push an imposed unit flow rate through the annulus, with interface position at ϕ_i . The lubrication scalings imply that the flow field is effectively one dimensional. Continuity of pressure at the interface means that the same pressure gradient acts in the axial direction in each fluid layer, but is modified in each fluid by the different densities. Flow rate generally increases with pressure gradient and hence we can find a (unique) pressure gradient that gives us a unit flow rate through the annulus at each depth, for the given interface position.

Given each $A(\phi_i(z, \tilde{t}))$, we can reconstruct Ψ from (3.21) and (3.22), by integrating with respect to ϕ from $\phi = 0$, where the boundary condition, $\Psi(0, z, \tilde{t}) = 0$, is applied. Recall that Ψ is continuous at the interface. Thus, the lubrication solution has the following leading-order dependency:

$$\Psi(\phi, z, \tilde{t}) \sim \Psi(\phi, \phi_i(z, \tilde{t})), \quad P(\phi, z, \tilde{t}) \sim P(\phi_i(z, \tilde{t})),$$

or equivalently

$$\Psi(\phi, z, \tilde{t}) \sim \Psi(\phi, \Phi_i(z, \tilde{t})), \quad P(\phi, z, \tilde{t}) \sim P(\Phi_i(z, \tilde{t})),$$

and the flux function $q(\Phi_i)$ is well defined, as the first term in (3.20).

3.2. Displacement classification

The lubrication model consists of (3.11), with $q(\Phi_i)$ defined from the solution of (3.20), using (3.22) and (3.21), at each depth z . Equation (3.11) is hyperbolic and gives the speed of propagation of the interface, W_i . In the absence of shocks, the interface speed is simply the characteristic speed:

$$W_i = \frac{dq}{d\Phi_i} = q'(\Phi_i). \quad (3.23)$$

When shocks occur, this definition must be modified, as we discuss below. We denote the wide ($\Phi_i = 0$) and narrow ($\Phi_i = 1$) side interface velocities by $W_{i,w}$ and $W_{i,n}$, respectively, and classify the displacement according to the values of $W_{i,w}$ and $W_{i,n}$, as follows.

(a) *Steady*. If $W_{i,w} \leq W_{i,n} \neq 0$, this indicates that a finger-like interface will become less elongated with time, and therefore that the assumptions underlying the lubrication approach will eventually become invalid. Effectively, this says that an elongating wide-side finger cannot exist. We classify this displacement as steady, noting that a type of global stability is implicit, i.e. interface elongation is bounded.

(b) *Unsteady*. If $W_{i,w} > W_{i,n} \neq 0$, the displacement is classified as unsteady. The interface moves faster on the wide side than the narrow side and the finger-like interface that we have assumed continues to elongate.

[†] For each ϕ , the expressions for the integrands, $\partial \Psi / \partial \phi$ in (3.22) and (3.21), are monotone, but not strictly monotone, since when unyielded at ϕ there is a range of A for which the fluid does not move. However, to satisfy (3.20), it is necessary that the fluids are moving for at least some finite range of ϕ . This gives strict monotonicity of the integral and hence a unique solution, $A(\phi_i)$.

(c) *Static channel.* If $W_{i,n} = 0$, then a static mud channel occurs on the narrow side of the annulus, since the interface is not moving there. The wide-side interface will be moving and a finger-like interface continues to elongate.

We see that the interface speed depends on the shape of $q(\Phi_i)$. The function $q(\Phi_i)$ varies smoothly from $q(0) = 0$ to $q(1) = 1$. In the absence of any density difference, ($b = 0$), we can see from (3.21) and (3.22) that (3.20) can only be solved if $A(\Phi_i) > 0$ and hence $q \geq 0$. Little else is obvious, *a priori*, and in general we must compute $q(\Phi_i)$ numerically. The dependency of $q(\Phi_i)$ is on the six rheological parameters, the eccentricity of the annulus and the buoyancy parameter (density difference between the two fluids).

3.2.1. Shock formation

When shocks occur, their speed of propagation can be calculated from mass conservation considerations (effectively the Rankine–Hugoniot conditions). Of primary interest is whether a shock occurs on the wide or narrow side of the annulus, since this modifies the definition of $W_{i,w}$ and/or $W_{i,n}$ from that in (3.23). It may be possible for other forms of shock to occur, but in this paper we confine our attention to wide-side and narrow-side shocks.

(i) *Shock on wide side.* Here, the wide-side interface velocity, computed from (3.23), is not the fastest interface velocity. The interface consequently steepens into a shock, which encompasses the wide side $\Phi_i = 0$. This results in a jump: $\Phi_i \in [0, \Phi_{i,w}]$, where $\Phi_{i,w}$ is the height of the propagating shock. The shock propagates at speed $W_{i,ws}$. Mass conservation dictates:

$$q(\Phi_i = \Phi_{i,w}) = \Phi_{i,w} W_{i,ws}. \quad (3.24)$$

Secondly, continuity of the interface velocity from above gives:

$$W_{i,ws} = q'(\Phi_i \rightarrow \Phi_{i,w}^+). \quad (3.25)$$

These two equations must be solved to find $\Phi_{i,w}$ and $W_{i,ws}$.

(ii) *Shock on narrow side.* Here the narrow-side interface velocity, computed from (3.23), is not the slowest interface velocity. The interface therefore steepens into a shock, which results in a jump, $\Phi_i \in [\Phi_{i,n}, 1]$. Denoting the shock height by $1 - \Phi_{i,n}$, and speed by $W_{i,ns}$, we obtain as before:

$$1 - q(\Phi_i = \Phi_{i,n}) = W_{i,ns}(1 - \Phi_{i,n}), \quad (3.26)$$

$$W_{i,ns} = q'(\Phi_i \rightarrow \Phi_{i,n}^-), \quad (3.27)$$

which we solve for $W_{i,ns}$ and $\Phi_{i,n}$.

Having found $W_{i,ws}$ and/or $W_{i,ns}$, we examine whether there is any interference between the two shocks and then re-define:

$$W_{i,w} = W_{i,ws}, \quad W_{i,n} = W_{i,ns},$$

accordingly, to give the correct interface propagation speed(s). It is often necessary to compute $q(\Phi_i)$ in order to examine whether shocks occur and to classify a displacement completely. However, no shocks can occur if q'' is of one sign. If $q'' > 0$ everywhere, then q' is increasing and q is strictly convex. Thus, the speed of the interface on the wide side of the annulus is $W_{i,w} = q'(0)$, which is strictly less than the speed on the narrow side, $W_{i,n} = q'(1)$. Thus, such displacements are classified as steady. Similarly, if $q'' < 0$ everywhere, then q' is decreasing, q is strictly concave. The interface becomes increasingly elongated and the displacement is classified as unsteady. Conversely, shocks do occur if q'' changes sign for $\Phi_i \in (0, 1)$.

3.3. Sufficient conditions for unsteady displacements

Wide- and narrow-side shocks do occur, (as we shall see later). However, the effect of a shock is to increase the wide-side interface velocity or decrease the narrow-side interface velocity, i.e.

$$W_{i,ws} \geq q'(0), \quad W_{i,ns} \leq q'(1). \quad (3.28)$$

Consequently, the condition

$$q'(0) > q'(1), \quad (3.29)$$

provides a sufficient condition for the displacement to be unsteady. Although possibly conservative, the expressions for $q'(0)$ and $q'(1)$ are relatively easy to compute and have a simple physical interpretation.

Finding $q'(0)$: Compute the wide-side pressure gradient, A_w , from:

$$1 = \int_0^1 \frac{\partial \Psi}{\partial \phi} \Big|_{k=2} d\phi.$$

Then, using (3.21) for $\partial \Psi / \partial \phi$ in fluid 1, and setting $H = 1 + e$, define $q'(0)$ by:

$$q'(0) = \frac{1}{1+e} \frac{\partial \Psi}{\partial \phi} (A_w) \Big|_{k=1}, \quad (3.30)$$

i.e. $q'(0)$ is the axial speed of fluid 1 on the wide side, but with the pressure gradient determined from an annulus full of fluid 2.

Finding $q'(1)$: Compute the narrow-side pressure gradient, A_n , from:

$$1 = \int_0^1 \frac{\partial \Psi}{\partial \phi} \Big|_{k=1} d\phi.$$

Then, using (3.22) for $\partial \Psi / \partial \phi$ in fluid 2, and setting $H = 1 - e$, define $q'(1)$ by:

$$q'(1) = \frac{1}{1-e} \frac{\partial \Psi}{\partial \phi} (A_n) \Big|_{k=2}, \quad (3.31)$$

i.e. $q'(1)$ is the axial speed of fluid 2 on the narrow side, but with the pressure gradient determined from an annulus full of fluid 1.

Thus, a sufficient condition for the evolution of an unsteady interface is that:

$$\frac{1}{1+e} \frac{\partial \Psi}{\partial \phi} (A_w) \Big|_{k=1} > \frac{1}{1-e} \frac{\partial \Psi}{\partial \phi} (A_n) \Big|_{k=2}. \quad (3.32)$$

3.4. Local interfacial stability and viscous fingering

Here, we attempt only a simplified analysis targeted at sufficient conditions for localized fingering to occur. Many localized analyses of Hele-Shaw displacement instabilities are based on a linear instability of a planar interface. Typically, the stability criteria that arise are analogous to those obtained by a more physically motivated approach, along the lines of the so-called Muskat approach (Muskat 1937). In the Muskat approach, one considers a (localized) long finger that extends ahead of the moving interface. The pressure gradient within the finger is determined by continuity from that in the external fluid. One then asks if the velocity of the fluid within the finger is faster than the speed of the fluid outside (implying instability to a finger propagating perpendicular to the interface). Here, we do not have a planar interface and linear stability analyses are consequently difficult. However, we may still adopt

the Muskat approach on the wide and narrow side, where the interface advances perpendicular to the wellbore axis.

Neglecting the possibility of shocks, we use the estimates (3.30) and (3.31) of the interface speed on the wide and narrow sides. On the wide side, the pressure gradient is A_w . According to the Muskat approach, a small finger of fluid 1 will grow ahead of the interface if:

$$\frac{1}{1+e} \frac{\partial \Psi}{\partial \phi}(A_w) \Big|_{k=1} > \frac{1}{1+e} \frac{\partial \Psi}{\partial \phi}(A_w) \Big|_{k=2}, \quad (3.33)$$

i.e. if the speed of fluid 1 within the finger is faster than that of fluid 2 outside the finger. Similarly, on the narrow side, a small finger of fluid 2 will grow, (backwards into fluid 1, behind the interface), if

$$\frac{1}{1-e} \frac{\partial \Psi}{\partial \phi}(A_n) \Big|_{k=2} < \frac{1}{1-e} \frac{\partial \Psi}{\partial \phi}(A_n) \Big|_{k=1}. \quad (3.34)$$

The approach behind the fingering instability criteria (3.33) and (3.34) is analogous to that adopted for planar displacements in porous media and Hele-Shaw cells. To see this, consider a vertical concentric annulus ($e=0$, $H=1$) for which there is a planar displacement front advancing at speed 1. Equations (3.33) and (3.34) are simply:

$$\frac{\partial \Psi}{\partial \phi}(A_w) \Big|_{k=1} > 1 = \frac{\partial \Psi}{\partial \phi}(A_n) \Big|_{k=1} \quad \text{or} \quad \frac{\partial \Psi}{\partial \phi}(A_n) \Big|_{k=2} < 1 = \frac{\partial \Psi}{\partial \phi}(A_w) \Big|_{k=2}.$$

However, note now that the relations (3.21) and (3.22) between A and $\partial \Psi / \partial \phi$ are strictly monotone and increasing if $\partial \Psi / \partial \phi > 0$. Therefore, viscous fingering occurs if:

$$A_w > A_n, \quad (3.35)$$

i.e. if the modified pressure gradient required for a unit areal flow rate of the displaced fluid 2, (A_w), is larger (implying less mobile) than the modified pressure gradient required for a unit areal flow rate of the displacing fluid 1, (A_n). Thus, the analysis is identical with the typical mobility ratio analysis, as in Pascal (1984*a, b*, 1986) and Coussot (1999).

3.5. Example results

The parameter space for our displacement model consists of the eccentricity $e \in [0, 1)$, the six positive rheological parameters: κ_1 , m_1 , $\tau_{1,Y}$, κ_2 , $m_2=2$, $\tau_{2,Y}$, and the buoyancy parameter b . A negative value of b implies that fluid 1 (displacing) is denser than fluid 2 (displaced), i.e. fluid 2 is pushed up the annulus by buoyancy. From (3.32)–(3.34), we can define parameter regimes in this eight-dimensional space that represent sufficient conditions for unsteady displacements and/or local instability to occur. Two examples are shown in figures 3 and 4. The parameter selections are arbitrary.

In figure 3, we observe that unsteadiness and eventually local instability of the interface result for decreasing $\tau_{1,Y}$ and for increasing m_1 . Both trends effectively make fluid 1 less viscous and more shear-thinning. As the buoyancy is increased, the regions of instability and unsteadiness decrease. In figure 4, we observe an increasing domain of unsteadiness and instability as the eccentricity is increased and as the rheological parameters $\tau_{2,Y}$ and κ_2 are increased, making fluid 2 more viscous. Both figures 3 and 4 suggest that it is likely that the interface becomes unsteady before it becomes locally unstable owing to fingering instabilities, i.e. local instability implies unsteadiness, but not vice versa. In the next section, we see that this can be established analytically for small eccentricities.

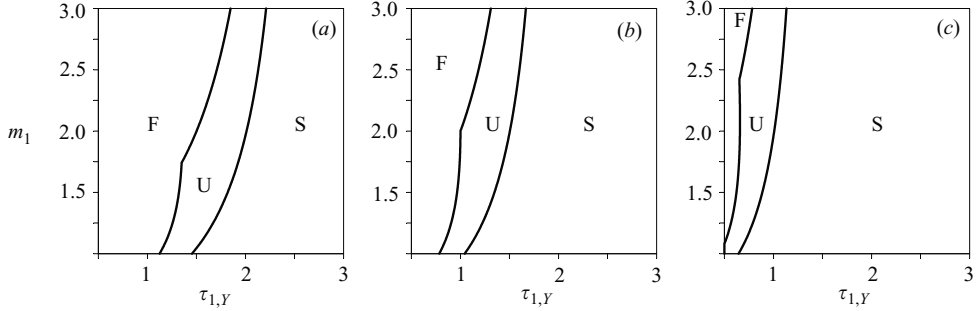


FIGURE 3. Example unsteady displacement and local instability/viscous fingering regimes: effects of changing $\tau_{1,Y}$ and m_1 for different buoyancy parameters: (a) $b=0.5$ (negative buoyancy, displaced fluid heavier than displacing); (b) $b=0$ (iso-density); (c) $b=-0.5$ (positive buoyancy, displaced fluid lighter than displacing). Fixed parameters are: $\tau_{2,Y}=1.0$, $\kappa_1=\kappa_2=0.5$, $m_2=2$, $e=0.2$. F, local fingering instability (3.33) or (3.34), and unsteady (3.32); U, unsteady (3.32), but no local instability; S, neither unsteady (3.32) nor local instability (3.33) or (3.34).

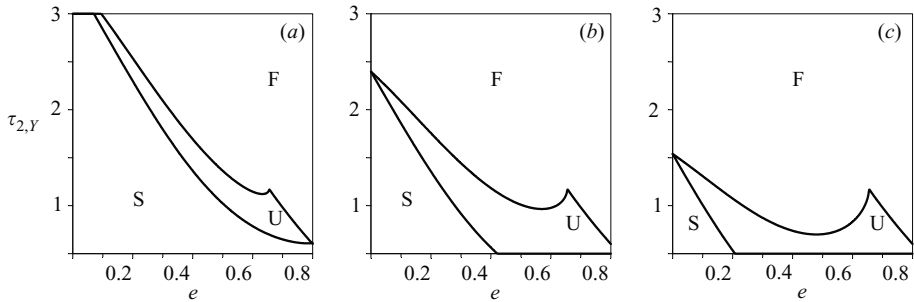


FIGURE 4. Example unsteady displacement and local instability/viscous fingering regimes: effects of changing $\tau_{2,Y}$ and e for different κ_2 : (a) $\kappa_2=0.5$; (b) $\kappa_2=1.0$; (c) $\kappa_2=1.5$. Fixed parameters are: $\tau_{1,Y}=1.0$, $\kappa_1=1.0$, $m_1=1$, $m_2=2$, $b=-0.5$. F, local fingering instability (3.33) or (3.34), and unsteady (3.32); U, unsteady (3.32), but no local instability; S, neither unsteady (3.32) nor local instability (3.33) or (3.34).

4. Analytical estimates for small eccentricity

The criteria (3.32)–(3.34) can be evaluated more explicitly in the case of small eccentricity, $e \ll 1$, and for simpler fluid models analytical expressions are even possible. Viscous fingering and unsteady displacements do not appear to have been considered for Newtonian and power law fluids in eccentric annuli, so these results appear to be novel, (i.e. as well as the results for the Herschel–Bulkley fluids). We use a regular perturbation method which we outline below (details are straightforward).

Our two main assumptions are that no shocks occur and that (since $e \ll 1$), the fluids are yielded for all values of Φ_i . We adopt a regular expansion for $A(\Phi_i)$, of form:

$$A(\Phi_i) \sim A_0(\Phi_i) + eA_1(\Phi_i) + e^2A_2(\Phi_i) + \dots,$$

where $A_0(\Phi_i)$ represents the modified pressure gradient for the concentric problem. It is straightforward to derive the following expansions in powers of $e \ll 1$.

$$\phi_i \sim \Phi_i - \frac{e}{\pi}S + \frac{e^2}{\pi}SC + \frac{e^3}{\pi}(S^3 - SC^2) + O(e^4), \quad (4.1)$$

$$H(\phi_i(\Phi_i)) \sim 1 + eC + e^2S^2 - \frac{3}{2}e^3S^2C + e^4(2S^2C^2 - \frac{7}{6}S^4) + O(e^5), \quad (4.2)$$

where $S = S(\Phi_i) = \sin \pi \Phi_i$ and $C = C(\Phi_i) = \cos \pi \Phi_i$. Equations (3.21) and (3.22) become, to $O(e)$:

$$\left. \frac{\partial \Psi}{\partial \phi} \right|_{k=1} \sim K(A_0, \tau_{1,Y}, m_1, \kappa_1) [1 + e A_1 r(\tau_{1,Y}, m_1, A_0) + e s(\tau_{1,Y}, m_1, A_0) \cos \pi \phi], \quad (4.3)$$

$$\left. \frac{\partial \Psi}{\partial \phi} \right|_{k=2} \sim K(A_0 - b, \tau_{2,Y}, m_2, \kappa_2) [1 + e A_1 r(\tau_{2,Y}, m_2, A_0 - b) + e s(\tau_{2,Y}, m_2, A_0 - b) \cos \pi \phi], \quad (4.4)$$

where

$$K(A, \tau_Y, m, \kappa) = \text{sgn}(A) \frac{(|A| - \tau_Y)^{m+1} (|A| + \tau_Y / (m + 1))}{\kappa^m (m + 2) |A|^2}, \quad (4.5)$$

$$r(\tau_Y, m, A) = \frac{m(m + 1) |A|^2 + 2m |A| \tau_Y + 2\tau_Y^2}{(|A| - \tau_Y) [(m + 1) |A| + \tau_Y] |A|}, \quad (4.6)$$

$$s(\tau_Y, m, A) = \frac{(m + 2)(m + 1) |A|^2}{(|A| - \tau_Y) [(m + 1) |A| + \tau_Y]}. \quad (4.7)$$

Substituting into (3.20) and expanding in powers of e , $A_0 = A_0(\Phi_i)$ is found at $O(1)$ as the solution of:

$$1 = K(A_0, \tau_{1,Y}, m_1, \kappa_1) \Phi_i + K(A_0 - b, \tau_{2,Y}, m_2, \kappa_2) (1 - \Phi_i), \quad (4.8)$$

Having found $A_0(\Phi_i)$, we write: $r_1(A_0) = r(\tau_{1,Y}, m_1, A_0)$, $r_2(A_0) = r(\tau_{2,Y}, m_2, A_0 - b)$, $s_1(A_0) = s(\tau_{1,Y}, m_1, A_0)$, $s_2(A_0) = s(\tau_{2,Y}, m_2, A_0 - b)$, $K_1(A_0) = K(A_0, \tau_{1,Y}, m_1, \kappa_1)$, $K_2(A_0) = K(A_0 - b, \tau_{2,Y}, m_2, \kappa_2)$ and find A_1 from the $O(e)$ terms in (3.20):

$$A_1(\Phi_i) = \frac{\sin \pi \Phi_i}{\pi} \frac{K_1(1 - s_1) - K_2(1 - s_2)}{r_1 K_1 \Phi_i + r_2 K_2 (1 - \Phi_i)}. \quad (4.9)$$

We then evaluate $q(\Phi_i)$ to $O(e)$, (after some algebra):

$$q(\Phi_i) \sim K_1 \Phi_i - e K_1 K_2 \frac{\sin \pi \Phi_i}{\pi} \left[\frac{\Phi_i r_1 (1 - s_2) + (1 - \Phi_i) r_2 (1 - s_1)}{r_1 K_1 \Phi_i + r_2 K_2 (1 - \Phi_i)} \right]. \quad (4.10)$$

We can differentiate this expression and evaluate at $\Phi_i = 0, 1$, for condition (3.32). Conditions (3.33) and (3.34) are evaluated from (4.3) and (4.4). We present this as the following pseudo-algorithm:

(a) Evaluate $A_w = A_0(0)$ and $A_n = A_0(1)$ from (4.8), i.e. solve the nonlinear equations:

$$1 = K_2(A_w), \quad 1 = K_1(A_n).$$

Note that these are identical with the definitions in §3.4, at $e = 0$.

(b) Evaluate the various wide- and narrow-side interface velocities and fluid velocities:

$$\begin{aligned} q'(0) &= K_1(A_w)(1 + e[s_1(A_w) - 1]), & q'(1) &= K_2(A_n)(1 - e[s_2(A_n) - 1]), \\ \left. \frac{\partial \Psi}{\partial \phi} \right|_{k=1}(0) &= K_1(A_w)[1 + e s_1(A_w)], & \left. \frac{\partial \Psi}{\partial \phi} \right|_{k=1}(1) &= K_1(A_n)[1 - e s_1(A_n)], \\ \left. \frac{\partial \Psi}{\partial \phi} \right|_{k=2}(0) &= K_2(A_w)[1 + e s_2(A_w)], & \left. \frac{\partial \Psi}{\partial \phi} \right|_{k=2}(1) &= K_2(A_n)[1 - e s_2(A_n)]. \end{aligned}$$

(c) Condition (3.32) for an unsteady displacement front, becomes:

$$K_1(A_w)(1 + e[s_1(A_w) - 1]) > K_2(A_n)(1 - e[s_2(A_n) - 1]). \quad (4.11)$$

(d) The conditions for wide- and narrow-side local instabilities are, respectively:

$$K_1(A_w)[1 + es_1(A_w)] > K_2(A_w)[1 + es_2(A_w)], \quad (4.12)$$

$$K_1(A_n)[1 - es_1(A_n)] > K_2(A_n)[1 - es_2(A_n)]. \quad (4.13)$$

Note that $K_2(A_w) = K_1(A_n) = 1$, so that when $e = 0$ both (4.12) and (4.13) can be combined into one inequality and this coincides with (4.11), i.e. the criteria for unsteady interfaces and viscous fingering are the same in a concentric annulus. For $e > 0$, it is necessary to consider particular fluids.

4.1. Newtonian fluids

We assume both fluids are Newtonian and that

$$|b| < |A_0(\Phi_i)|, \quad \forall \Phi_i, \quad (4.14)$$

which ensures that $\text{sgn}(A_0) = \text{sgn}(A_0) = 1$. We define $\lambda = \kappa_1/\kappa_2$ and $\delta = -b/(3\kappa_2)$, representing the viscosity ratio and a buoyancy parameter, respectively. We find $r_1 = r_2 = 1/A_0$, $s_1 = s_2 = 3$,

$$K_1 = \frac{1 - \delta(1 - \Phi_i)}{\Phi_i + \lambda(1 - \Phi_i)}, \quad K_2 = \frac{\lambda + \delta\Phi_i}{\Phi_i + \lambda(1 - \Phi_i)},$$

and thus,

$$q(\Phi_i) \sim \frac{1 - \delta(1 - \Phi_i)}{\Phi_i + \lambda(1 - \Phi_i)}\Phi_i + \frac{2e \sin \pi\Phi_i}{\pi} \frac{[\lambda + \delta\Phi_i][1 - \delta(1 - \Phi_i)]}{[\Phi_i + \lambda(1 - \Phi_i)]^2}. \quad (4.15)$$

The wide- and narrow-side interface velocities are therefore:

$$q'(0) \sim \frac{(1 - \delta)(1 + 2e)}{\lambda}, \quad q'(1) \sim (\lambda + \delta)(1 - 2e),$$

and the differential velocity is

$$q'(0) - q'(1) \sim \frac{(1 - \delta)}{\lambda} - (\lambda + \delta) + 2e \left[\frac{(1 - \delta)}{\lambda} + \lambda + \delta \right].$$

Assuming small positive δ , we note that non-zero eccentricity always promotes a positive differential velocity. In the event that $\delta = 0$, we have

$$q'(0) - q'(1) \sim \frac{1}{\lambda} - \lambda + 2e \left[\frac{1}{\lambda} + \lambda \right],$$

and sufficient condition for an unsteady displacements is found when the eccentricity satisfies:

$$e \geq \frac{1}{2} \left(\frac{\lambda^2 - 1}{\lambda^2 + 1} \right), \quad (4.16)$$

i.e. for a steady-state displacement it is always necessary that the displacing fluid is more viscous than the displaced. With buoyancy, this generalizes to

$$e \geq \frac{1}{2} \left(\frac{\lambda^2 - 1 + \delta(\lambda + 1)}{\lambda^2 + 1 + \delta(\lambda - 1)} \right). \quad (4.17)$$

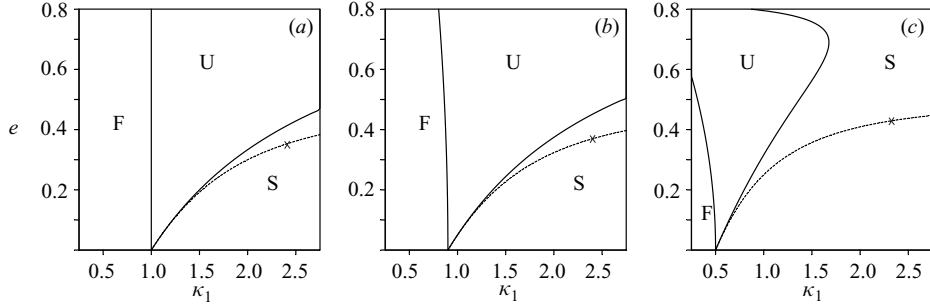


FIGURE 5. Unsteady displacement and viscous fingering regimes for Newtonian fluids, comparison with (4.17), (dashed line, marked with a \times). Effects of changing κ_1 and e for different $\delta = -b/(3\kappa_2)$: (a) $\delta = 0$; (b) $\delta = 0.1$; (c) $\delta = 0.5$. Fixed parameters are: $\tau_{1,Y} = \tau_{2,Y} = 0$, $\kappa_2 = 1.0$, $m_1 = m_2 = 1$.

We note that the numerator in (4.17) increases faster with δ than the denominator. Thus, a positive δ (negative b) apparently increases the eccentricity required for an unsteady displacement (at least for small e).

In figure 5 we plot the regimes for an unsteady displacement, (3.32), and for viscous fingering, (3.33) and (3.34), for Newtonian fluids. We make a comparison against the analytical expression (4.17), for different values of δ . As commented above, an increased buoyancy parameter serves to compensate for eccentricity. For small eccentricity, the computed results are observed to coincide with the plotted curve (4.17).

4.2. Power-law fluids

We again assume that $|b|$ is sufficiently small for (4.14) to hold. We do not attempt to find an analytical expression for $q(\Phi_i)$, although this appears possible for certain integer values of the inverse power-law indices, m_k . Computing $q'(0)$ and $q'(1)$ directly:

$$q'(0) \sim \frac{[\kappa_2(m_2 + 2)^{1/m_2} + b]^{m_1}}{\kappa_1^{m_1}(m_1 + 2)} [1 + (m_1 + 1)e],$$

$$q'(1) \sim \frac{[\kappa_1(m_1 + 2)^{1/m_1} - b]^{m_2}}{\kappa_2^{m_2}(m_2 + 2)} [1 - (m_2 + 1)e].$$

The differential velocity is therefore:

$$q'(0) - q'(1) \sim \frac{[\kappa_2(m_2 + 2)^{1/m_2} + b]^{m_1}}{\kappa_1^{m_1}(m_1 + 2)} - \frac{[\kappa_1(m_1 + 2)^{1/m_1} - b]^{m_2}}{\kappa_2^{m_2}(m_2 + 2)} + e \left[\frac{[\kappa_2(m_2 + 2)^{1/m_2} + b]^{m_1}(m_1 + 1)}{\kappa_1^{m_1}(m_1 + 2)} + \frac{[\kappa_1(m_1 + 2)^{1/m_1} - b]^{m_2}(m_2 + 1)}{\kappa_2^{m_2}(m_2 + 2)} \right]. \quad (4.18)$$

A sufficient condition for an unsteady displacement is that the differential velocity above be positive. Setting $e = 0$ above, we recover the condition for a concentric annulus. Given in terms of the eccentricity, this becomes:

$$e > \frac{\frac{[\kappa_1(m_1 + 2)^{1/m_1} - b]^{m_2}}{\kappa_2^{m_2}(m_2 + 2)} - \frac{[\kappa_2(m_2 + 2)^{1/m_2} + b]^{m_1}}{\kappa_1^{m_1}(m_1 + 2)}}{\frac{[\kappa_1(m_1 + 2)^{1/m_1} - b]^{m_2}(m_2 + 1)}{\kappa_2^{m_2}(m_2 + 2)} + \frac{[\kappa_2(m_2 + 2)^{1/m_2} + b]^{m_1}(m_1 + 1)}{\kappa_1^{m_1}(m_1 + 2)}}. \quad (4.19)$$

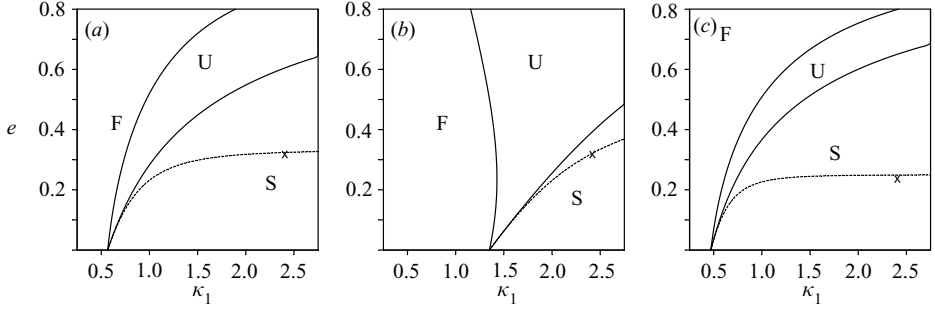


FIGURE 6. Unsteady displacement and viscous fingering regimes for power-law fluids, comparison with (4.19), (dashed line, marked with a \times). Effects of changing κ_1 and e for various m_1, m_2 : (a) $m_1 = 1.0, m_2 = 2.0$; (b) $m_1 = 2.0, m_2 = 1.0$; (c) $m_1 = 1.0, m_2 = 3.0$. Fixed parameters are: $\tau_{1,Y} = \tau_{2,Y} = 0.0, \kappa_2 = 1.0, b = 0.3$.

The conditions for local fingering on either the wide or narrow side of the annulus are:

$$\frac{[\kappa_2(m_2 + 2)^{1/m_2} + b]^{m_1}}{\kappa_1^{m_1}(m_1 + 2)} [1 + (m_1 + 2)e] > [1 + (m_2 + 2)e],$$

$$[1 - (m_1 + 2)e] > \frac{[\kappa_1(m_1 + 2)^{1/m_1} - b]^{m_2}}{\kappa_2^{m_2}(m_2 + 2)} [1 - (m_2 + 2)e].$$

Combining these, we can see that if fingering occurs on both the wide and narrow sides of the annulus, then the displacement front is unsteady, i.e. local instability implies an unsteady displacement for small e . However, an unsteady displacement apparently does not imply local instability of the interface. Figure 6 plots the regimes for an unsteady displacement, (3.29), and for viscous fingering, (3.33) and (3.34), for a range of different power-law fluid combinations, comparing against (4.19).

4.3. Yield stress fluids

In order to find $q'(0)$ and $q'(1)$, for fluids with positive yield stresses, analytic solution is not possible. However, finding A_w and A_n is straightforward. We again assume that $|b|$ is sufficiently small for (4.14) to hold. At $\Phi_i = 0$, $A_w - b$ is given by:

$$A_w - b = \tau_{2,Y} \Upsilon(m_2, B_2),$$

where $B_2 = \tau_{2,Y}/\kappa_2$, and $\Upsilon(m, B)$ is the root of $Q(\Upsilon, m, B) = 0$ for which $\Upsilon > 1$:

$$Q(\Upsilon, m, B) = (\Upsilon - 1)^{m+1} [(m + 1)\Upsilon + 1] - \Upsilon^2(m + 1)(m + 2)/B^m, \quad (4.20)$$

which is essentially a Buckingham equation for the concentric annular flow. It may be easily deduced that $Q(\Upsilon, m, B) = 0$ has a single root in $\Upsilon > 1 - 2^{1/m}/B$. Similarly, with $B_1 = \tau_{1,Y}/\kappa_1$, at $\Phi_i = 1$, we find that

$$A_n = \tau_{1,Y} \Upsilon(m_1, B_1).$$

We can conclude that for $e \ll 1$, the criterion (3.29) depends dimensionlessly on

$$(e, b/\tau_{2,Y}, \tau_{1,Y}/\tau_{2,Y}, m_1, m_2, B_1, B_2),$$

i.e. one of our eight dimensionless parameters is redundant.

Further, we have a similar result to the power law fluid, in that local instability implies that the displacement is unsteady, but not necessarily vice versa. To see this, note that if (4.12) and (4.13) hold, then

$$\frac{K_1(A_w)}{K_2(A_n)} > \frac{[1 + es_2(A_w)][1 - es_2(A_n)]}{[1 + es_1(A_w)][1 - es_1(A_n)]}.$$

Condition (4.11) for the unsteady displacement is therefore satisfied if

$$\frac{[1 + es_2(A_w)][1 - es_2(A_n)]}{[1 + es_1(A_w)][1 - es_1(A_n)]} > \frac{(1 - e[s_2(A_n) - 1])}{(1 + e[s_1(A_w) - 1])}.$$

Multiplying out and retaining only terms of $O(e)$, (4.11) follows when:

$$s_2(A_w) + s_1(A_n) > 2, \quad (4.21)$$

but this condition is always satisfied, since for $|A| > \tau_Y$, the lower bound $s > m + 2$ is easy to derive.

5. Iso-density displacements

We have seen in the previous section that local instability of the interface appears to occur only when the interface becomes unsteady, at least for small eccentricities. Thus, predicting the transition between steady and unsteady displacements has increased importance. To do this correctly in the context of the lubrication model, we must also consider the possible formation of shocks. To reduce the number of parameters that must be considered, we start by looking at iso-density displacements, $b = 0$. For such displacements $q(\Phi_i) \geq 0$. First, we consider pure advective dispersion in § 5.1, which always gives rise to an unsteady displacement. We then investigate how dispersion is countered by a rheology variation, in § 5.2. We explore a wide range of parameter variations.

5.1. Advection of a passive tracer

Consider the simple case for which the two fluids are identical. This corresponds to pure advection of a single fluid that is coloured say red/blue by a passive tracer above/below a certain interface. It is easiest to see what is happening analytically by first considering a power-law fluid, $\tau_Y = 0$, (we consider a yield stress fluid afterwards and the picture is qualitatively similar). Since the fluids are identical, it is clear that A does not vary with Φ_i . Hence, substituting (3.21) and (3.22) into (3.20), we find A as the solution of:

$$1 = \frac{A^m}{\kappa^m(m+2)} \int_0^1 H^{m+2} d\phi \quad (5.1)$$

and thus,

$$q(\Phi_i) = \frac{\int_0^{\phi_i(\Phi_i)} H^{m+2} d\phi}{\int_0^1 H^{m+2} d\phi}, \quad (5.2)$$

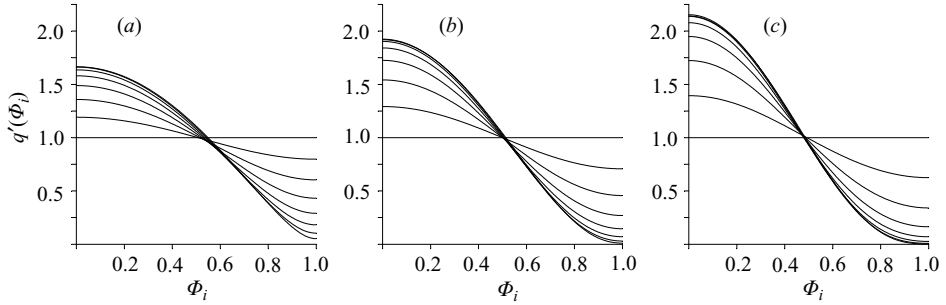


FIGURE 7. Interface propagation speed $W_i(\Phi_i) = q'(\Phi_i)$ for a power law fluid displacing itself, ($\kappa = 1$): (a) $m = 1$ (Newtonian); (b) $m = 2$; (c) $m = 3$. Each figure shows successive plots of $q'(\Phi_i)$ with increasing eccentricity: $e = 0, 0.1, 0.2, \dots, 0.7$.

and after a little algebra:[†]

$$W_i(\Phi_i) = q'(\Phi_i) = \frac{H^{m+1}(\phi_i(\Phi_i))}{\int_0^1 H^{m+2} d\phi}. \quad (5.3)$$

Since H decreases monotonically, it follows that there are no shocks, $W_{i,w} > W_{i,n}$, and the flow is always classified as unsteady (unless of course $e = 0$). In figure 7, we plot $W_i(\Phi_i) = q'(\Phi_i)$ for a range of m and e . In general, the separation of wide and narrow sides increases both with eccentricity and with m , both of which effects are intuitive. For large eccentricity, the interface velocity on the narrow side of the annulus approaches zero, (attained only at $e = 1$). For small eccentricities, using the previous expansions for H , we find that the interface will elongate at a speed:

$$W_{i,w} - W_{i,n} \sim 2e(m+1) - e^3 \frac{(m+1)(m^2 + 11m + 6)}{6} + O(e^5).$$

Comparison with the computed solutions in figure 7 is reasonable for $e \lesssim 0.25$.

The interface behaviour is qualitatively similar with a non-zero yield stress. We find that $q(\Phi_i)$ increases monotonically and that $q'(\Phi_i)$ decreases with Φ_i . Hence, again no shocks arise and $W_i(\Phi_i) = q'(\Phi_i)$ everywhere. As an example, in figure 8 we plot $W_i(\Phi_i) = q'(\Phi_i)$ for different m, κ and e , at a fixed $\tau_Y = 1$. All rheological combinations are classified as unsteady, in that the wide-side and narrow-side interface positions will separate steadily, but now it is also possible for the narrow side to be unyielded at higher values of the eccentricity. This is observable in each of figures 8(a) to 8(c), at high eccentricities, where $q'(\Phi_i) = 0$, over some range of Φ_i close to 1. As before,

[†] Remarks: (i) For identical fluids in a uniform annulus, we are able to find a one-dimensional axial velocity solution to (2.4). For a purely axial velocity, the lubrication assumptions are obviously satisfied, and so are the boundary conditions on Ψ . According to Pelipenko & Frigaard (2004a), there exists a unique solution to this problem and therefore the axial (lubrication) solution is also the exact solution to the full two-dimensional problem. As a familiar analogy, consider for example a passive tracer advected in a Poiseuille flow. The Poiseuille flow is a solution to the full Stokes (and Navier–Stokes) equations. (ii) It may seem strange that the consistency κ does not enter into (5.3), although the shear-thinning index does. This is, however, analogous to the situation in, for example, advection of a passive tracer in Hagen–Poiseuille flow. The viscosity does not influence the (dimensionless) velocity profile in a Newtonian fluid pipe flow and neither would the consistency with a power-law fluid, i.e. this result is simply due to the invariance of the velocity profile shape with κ for a fixed flow rate; only e and m affect the velocity distribution around the annulus.

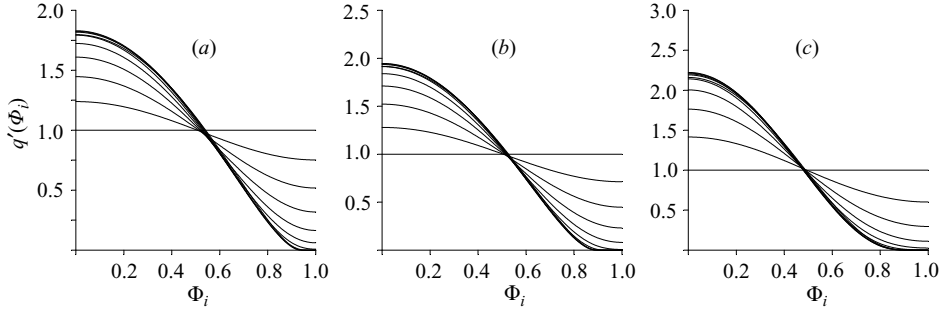


FIGURE 8. Interface propagation speed $W_i(\Phi_i) = q'(\Phi_i)$ for a yield stress fluid displacing itself: (a) $m = 1$, $\kappa = 1$, $\tau_Y = 1$ (Bingham); (b) $m = 1$, $\kappa = 0.5$, $\tau_Y = 1$; (c) $m = 2$, $\kappa = 1$, $\tau_Y = 1$. Each figure shows successive plots of $q'(\Phi_i)$ with increasing eccentricity: $e = 0, 0.1, 0.2, \dots, 0.9$.

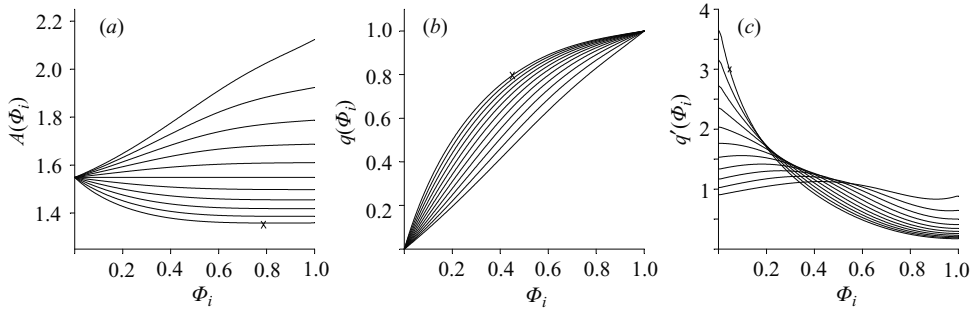


FIGURE 9. Effects of increasing m_1 (displacing fluid is increasingly shear-thinning): (a) $A(\Phi_i)$; (b) $q(\Phi_i)$; (c) $q'(\Phi_i)$. Fixed parameters: $\tau_{1,Y} = \tau_{2,Y} = 0.5$, $\kappa_1 = \kappa_2 = 0.5$, $m_2 = 2$, $e = 0.2$, $b = 0$. Inverse index $m_1 = 1.0, 1.2, 1.4, \dots, 3.0$; $m_1 = 3.0$ is marked with a \times .

increasing eccentricity increases the wide–narrow side differential velocity, $W_{i,w} - W_{i,n}$. Lowering the consistency κ (figure 8b) increases the differential velocity and allows for a thicker unyielded channel on the narrow side. Increasing m (figure 8c) also increases the differential velocity and unyielded channel on the narrow side.

5.2. Effects of rheological variations on dispersion

As we have seen above, without any difference in physical properties between the two fluids, the displacement is always unsteady, leading to pure advective dispersion along the length of the well. To examine the effects of the different parameters on advective dispersion, we fix the properties of the displaced fluid 2 (at $\tau_{2,Y} = 0.5$, $\kappa_2 = 0.5$, $m_2 = 2$), also fix $e = 0.2$, and vary each of m_1 , $\tau_{1,Y}$ and κ_1 in turn. The results are shown in figures 9–11, in which we have computed $A(\Phi_i)$, $q(\Phi_i)$ and $q'(\Phi_i)$.

In each of figures 9(a)–11(a), the modified pressure gradient $A(\Phi_i)$ varies monotonically with Φ_i . This is expected. As Φ_i increases, a larger fraction of the annulus contains fluid 1. If fluid 1 is more viscous than fluid 2, the pressure gradient needed to pump a unit flow rate of both fluids will increase, and vice versa if fluid 1 is less viscous. Since for these examples, we only vary one rheological parameter at a time from our base case there is no confusion here, i.e. it might be possible to choose different rheological parameters such that the two fluids are not definitively more or less viscous than one another.

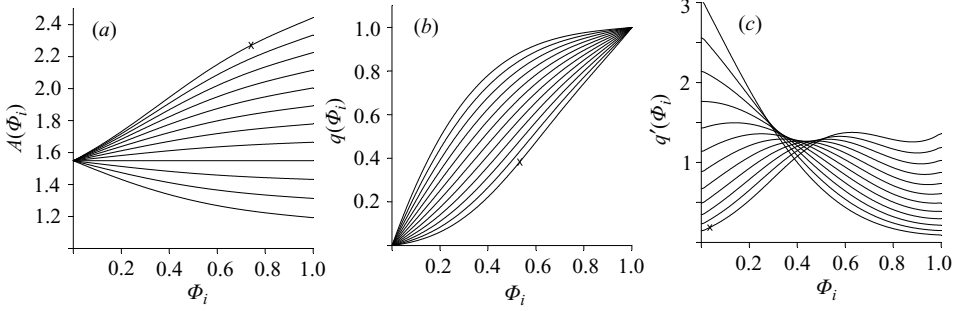


FIGURE 10. Effects of increasing $\tau_{1,Y}$ (displacing fluid yield stress): (a) $A(\Phi_i)$; (b) $q(\Phi_i)$; (c) $q'(\Phi_i)$. Fixed parameters: $\tau_{2,Y}=0.5$, $\kappa_1=\kappa_2=0.5$, $m_1=m_2=2$, $e=0.2$, $b=0$. Yield stress $\tau_{1,Y}=0.2, 0.3, 0.4, \dots, 1.3$; $\tau_{1,Y}=1.3$ is marked with a \times .

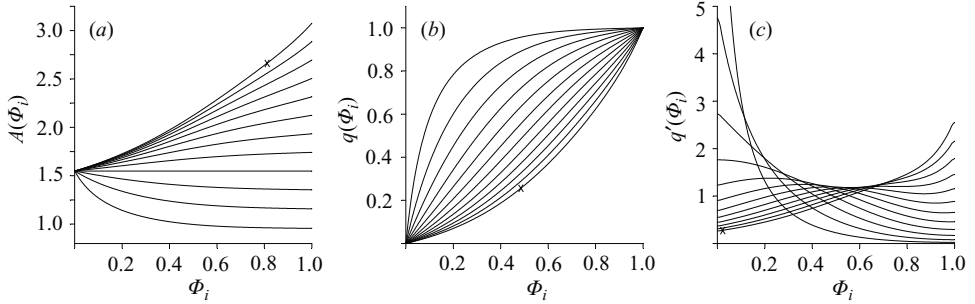


FIGURE 11. Effects of increasing κ_1 (displacing fluid consistency): (a) $A(\Phi_i)$; (b) $q(\Phi_i)$; (c) $q'(\Phi_i)$. Fixed parameters: $\tau_{1,Y}=\tau_{2,Y}=0.5$, $\kappa_2=0.5$, $m_1=m_2=2$, $e=0.2$, $b=0$. Consistency $\kappa_1=0.2, 0.3, 0.4, \dots, 1.3$; $\kappa_1=1.3$ is marked with a \times .

Figures 9(b)–11(b) each show a monotone increase in $q(\Phi_i)$ with Φ_i . The variations in $q'(\Phi_i)$ with each of m_1 , $\tau_{1,Y}$ and κ_1 (figures 9c–11c) are more relevant to the displacement type. For large m_1 (figure 9c), $q'(\Phi_i)$ decreases monotonically. The flow is unsteady with a large differential velocity and no shocks. As m_1 decreases through m_2 , $q'(\Phi_i)$ ceases to be monotone: $q'(0)$ is not the fastest characteristic speed and $q'(1)$ is not the slowest characteristic speed. Shocks appear on both the wide and narrow sides of the annulus. Their positions and speeds must be calculated (as described in §3.2) in order to determine the wide- and narrow-side interface propagation speeds. The shocks do not appear simultaneously on wide and narrow sides. Initially, the two shock positions are distinct and the wide-side shock moves faster than the narrow side (unsteady displacement). As m_1 decreases, the shocks meet in the centre and we arrive at a steady displacement. The above transition from unsteady to steady also occurs in figure 10(c), as $\tau_{1,Y}$ increases, and in figure 11(c), as κ_1 increases. In each case, the transition from unsteady to steady occurs as the displacing fluid becomes sufficiently more viscous than the displaced fluid, as is indeed physically intuitive. At the small selected eccentricity, $e=0.2$, we do not see a transition to the static narrow-side channel. We illustrate the above transition from unsteady dispersion to shocks and eventually to a steady state in figure 12. The wide-side shock appears just above $\kappa_1=0.5$ and the narrow-side shock at around $\kappa_1=0.65$. The two shocks move steadily together and coalesce into a steady displacement at approximately $\kappa_1=0.864$.

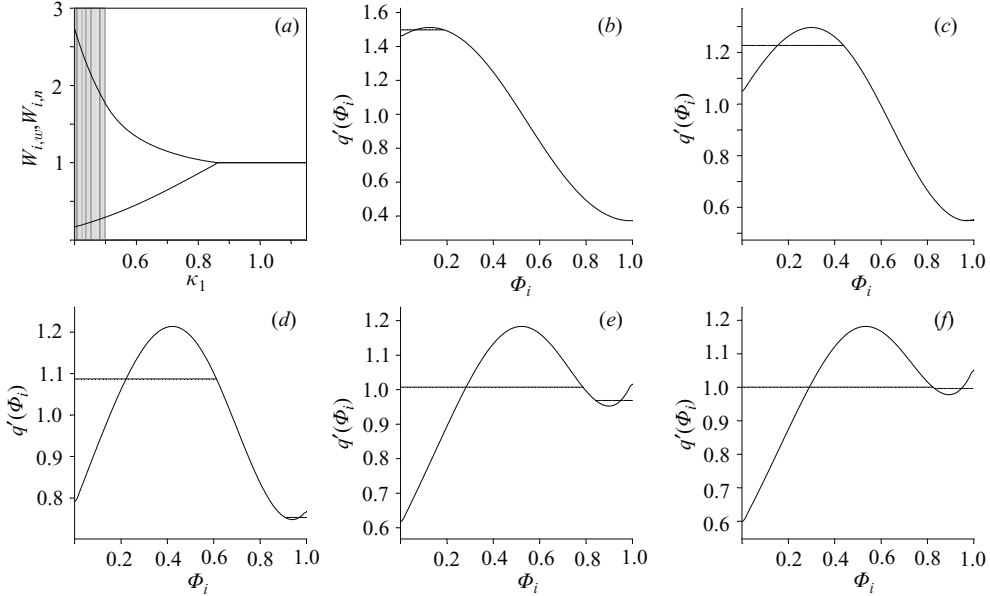


FIGURE 12. Effects of increasing κ_1 on $W_{i,w}$ and $W_{i,n}$: (a) variations in $W_{i,w} \geq W_{i,n}$, the shaded area denotes the range where there are no shocks; (b) $\kappa_1 = 0.55$, a shock emerges on the wide side; (c) $\kappa_1 = 0.65$, the narrow-side shock appears; (d) $\kappa_1 = 0.75$, the shocks grow towards each other; (e) $\kappa_1 = 0.85$; (f) $\kappa_1 = 0.863$, just prior to the shocks meeting. In the absence of shocks, $W_{i,w}$ and $W_{i,n}$ are simply the wide- and narrow-side values of $q'(\Phi_i)$. When shocks occur, the velocities $W_{i,w}$ and $W_{i,n}$ are given by the horizontal dashed lines. Fixed parameters: $\tau_{1,Y} = \tau_{2,Y} = 0.5$, $\kappa_2 = 0.5$, $m_1 = m_2 = 2$, $e = 0.2$, $b = 0$.

In figure 13, we plot the evolving interface for the cases $\kappa_1 = 0.45$ (no shocks, unsteady), $\kappa_1 = 0.85$ (shocks, unsteady) and $\kappa_1 = 0.9$ (merged shocks, steady). The latter two values lie close either side of the transition to a steady displacement. Without shocks the elongation of the interface in figure 13(a) is very rapid. The difference between figures 13(b) and 13(c) is quite noticeable. Even very close to stability, the interface elongates in a discernible way, whereas immediately after the transition to stability, the interface propagates at steady unit speed across the annulus.

The computational method used for figure 13 is as follows. First, we construct $q'(\Phi_i)$ by solving (3.20) computationally for $N_{\Phi_i} = 100$ evenly spaced values of $\Phi_i \in [0, 1]$ and by using linear interpolation. Equation (3.11) is integrated from initial conditions of a horizontal interface. The method we use for (3.11) is due to Cockburn & Shu (1994) and is a compact differencing scheme that is nonlinearly stable and third-order in both time and space. The method in Cockburn & Shu (1994) is designed to be shock-capturing. Apart from the test-problems in Cockburn & Shu (1994), this method has been used previously in Fenie & Frigaard (1999) and Allouche, Frigaard & Sona (2000), for a similar problem of interface propagation with shock discontinuities and was found to perform well. The mesh discretization in the z -direction is $\Delta z = 0.02$. Although there is some numerical diffusion, at $\Phi_i = 0$ and $\Phi_i = 1$, the amount is limited as the interface evolves and the evolving wide-side shock is quite clear in figure 13(b). In general, the narrow-side shocks are hard to observe in such simulations since the wide-side shock moves steadily ahead and on the narrow side, the interface contours are compressed.

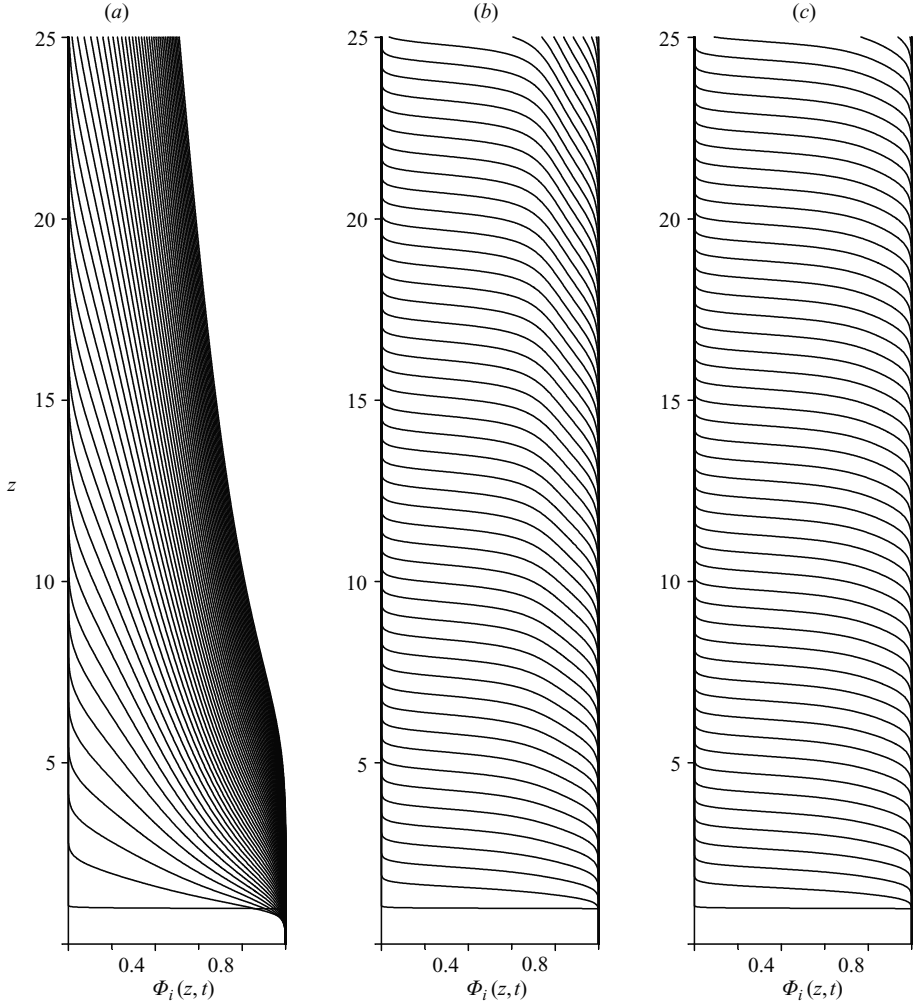


FIGURE 13. Transient displacement profiles at successive times for different κ_1 : (a) $\kappa_1 = 0.45$ (unsteady, no shocks); (b) $\kappa_1 = 0.85$ (unsteady with wide and narrow side shocks); (c) $\kappa_1 = 0.9$ (steady, coalesced shocks). Surfaces are plotted at time intervals $t = 0.5$. Fixed parameters: $\tau_{1,Y} = \tau_{2,Y} = 0.5$, $\kappa_2 = 0.5$, $m_1 = m_2 = 2$, $e = 0.2$, $b = 0$.

6. Effects of buoyancy on lubrication displacements

Intuitively, we expect buoyancy ($b < 0$) to aid displacement, and we shall see that this is generally the case. However as before, we first consider the effect of buoyancy on a passive tracer displacement.

6.1. Stabilization of passive tracer advection

We start with the passive tracer scenario, of identical rheologies, and look at the effects of slowly decreasing b from zero. In figure 14, we show typical variations in $A(\Phi_i)$, $q(\Phi_i)$ and $q'(\Phi_i)$. In figure 14(b) we see that $q(\Phi_i)$ is increasingly suppressed on the wide side of the annulus, as the buoyancy increases (i.e. as b decreases). As with the increase in displacing fluid rheology, we see initially that there are no shocks, but simply unsteady displacements. For larger negative b , shocks form on the wide and narrow sides. These coalesce at still larger negative b and the displacement stabilizes.

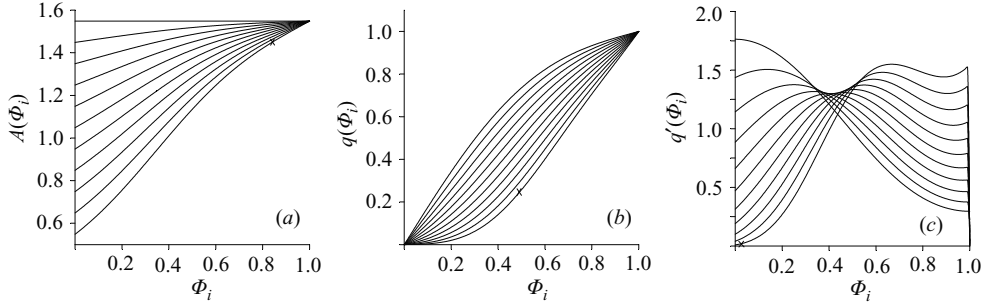


FIGURE 14. Effects of decreasing b (buoyancy parameter), on passive tracer advection: (a) $A(\Phi_i)$; (b) $q(\Phi_i)$; (c) $q'(\Phi_i)$. Fixed parameters: $\tau_{1,Y} = \tau_{2,Y} = 0.5$, $\kappa_1 = \kappa_2 = 0.5$, $m_1 = m_2 = 2$, $e = 0.2$. Buoyancy parameter: $b = 0, -0.1, -0.2, \dots, -1$; $b = -1$ is marked with a \times .

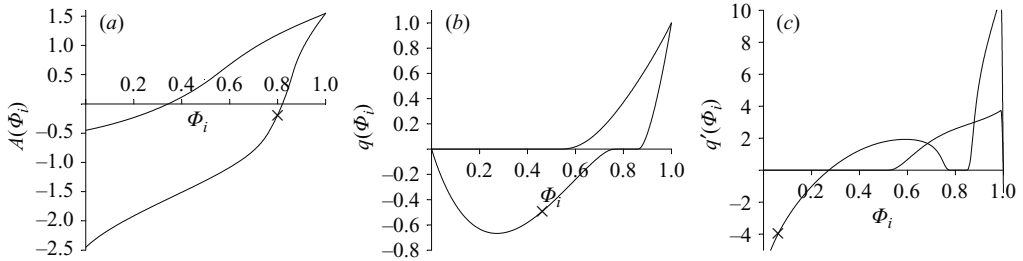


FIGURE 15. Effects of large negative b (buoyancy parameter), on passive tracer advection: (a) $A(\Phi_i)$; (b) $q(\Phi_i)$; (c) $q'(\Phi_i)$. Fixed parameters: $\tau_{1,Y} = \tau_{2,Y} = 0.5$, $\kappa_1 = \kappa_2 = 0.5$, $m_1 = m_2 = 2$, $e = 0.2$. Buoyancy parameter: $b = -2, -4$.

In a sense then, the effect of increasing buoyancy parallels that of increasing the displacing fluid effective viscosity.

At larger negative values of b , the suppression of $q(\Phi_i)$ for small Φ_i , seen in figure 14(b), becomes extreme. At a critical value of $b < 0$, we begin to see zero and eventually negative $q(\Phi_i)$, over a range of Φ_i close to the wide side, $\Phi_i = 0$. To understand this effect physically, note that the buoyancy parameter induces a jump in the axial pressure gradient driving the two fluids. For large negative b , this jump becomes so extreme that the only way to continue to satisfy the unit volumetric flow constraint is if the flow in the displacing fluid is zero, or eventually even negative. Two examples are shown in figure 15, for $b = -2$, $b = -4$. The range of Φ_i for which $q(\Phi_i) = 0$ corresponds to a range of modified pressure gradients $A(\Phi_i)$, for which $A(\Phi_i)$ is too small to move fluid 1; in this range, $A(\Phi_i)$ changes sign, changing from pushing fluid 1 downwards to upwards, but is unable to exceed the yield stress at the walls. This is verifiable numerically. Without a yield stress in fluid 1, the transition from positive to negative $q(\Phi_i)$ occurs at a single position where $A(\Phi_i) = 0$. For these extremely buoyant flows, the narrow-side interfacial velocity is evidently greater than that on the wide side, shocks form and the displacements are classified as steady.

6.2. Competition between rheology and buoyancy

In practice, we may be restricted in the use of either certain rheologies or densities. Thus, it is of interest to know whether a displacement can be made steady, by compensating either an adverse rheology difference with buoyancy, or an adverse

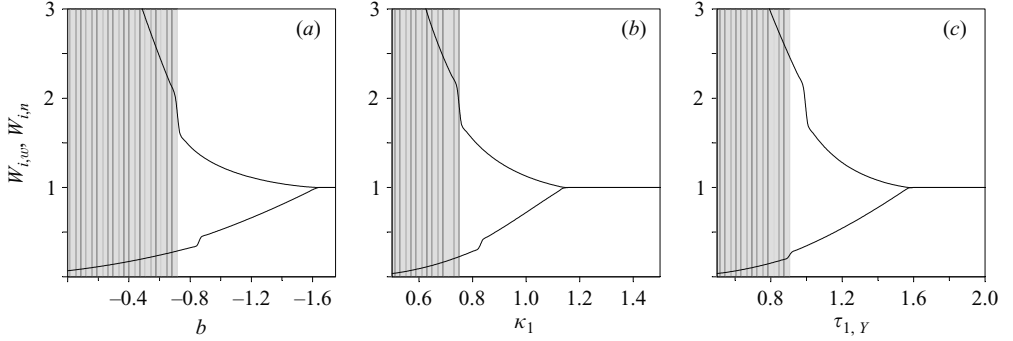


FIGURE 16. Coalescence of wide- and narrow-side shock speeds, $W_{i,w}$ and $W_{i,n}$: (a) buoyancy stabilizing rheology: $\tau_{1,Y}=0.4$, $\tau_{2,Y}=0.5$, $\kappa_1=0.5$, $\kappa_2=0.8$, $m_1=m_2=2$, $e=0.2$; (b) fluid 1 consistency stabilizing negative buoyancy: $b=0.5$, $\tau_{1,Y}=0.5=\tau_{2,Y}=0.5$, $\kappa_2=0.5$, $m_1=m_2=2$, $e=0.2$; (c) fluid 1 yield stress stabilizing negative buoyancy: $b=0.5$, $\tau_{2,Y}=0.5$, $\kappa_1=\kappa_2=0.5$, $m_1=m_2=2$, $e=0.2$.

buoyancy difference with rheology. In figure 16, we show that this is indeed the case. We compute the interface velocity on the wide and narrow sides, for three different scenarios in which an unsteady flow is stabilized, by competing rheological effects against buoyancy effect or vice versa. In general, the direction in which rheological or buoyancy parameters need be increased is wholly intuitive.

7. Comparison with industrial design criteria

There are two main advantages of using the lubrication model to determine whether or not there is a steady displacement. One is computational speed and simplicity, as compared to other computational methods such as fully two-dimensional or three-dimensional simulations. This allows determination of multi-parameter stability regimes and allows various optimization procedures to be implemented. The second is that close to a marginally stable parameter set, a simulation will converge progressively slowly to a stable steady state, i.e. simulation is simply unsuitable. Over the years, a number of criteria have been developed within the oilfield cementing industry, to act as design rules for a successful primary cementing job. It is our intention in this section to review some of these and make a comparison against predictions of the lubrication model.

In practice, different operating companies have different sets of design rules, that are either wholly or partly confidential. Thus, only a partial review is possible and we focus on just two representative systems of rules that are in the public domain. At the outset, it must also be mentioned that many cementing jobs are carried out in the turbulent regime, (meaning that all fluids pumped are turbulent, all around the annulus), and we do not address this here. We focus on purely laminar displacements. It is also evident that there will be ranges of flow rate for which neither wholly laminar nor wholly turbulent flows are found. Lastly, there are numerous operating guidelines that have little or no bearing on the fluid mechanics of mud displacement, e.g. control of cement setting times through retarders.

7.1. Lockyear et al.'s design criteria

The design system presented by Lockyear & Hibbert (1989) and Lockyear, Ryan, & Gunningham (1989) identifies three main requirements for a successful cementing job:

(a) *Mud displacement.* The drilling mud (displaced fluid) gel must be broken during mud circulation, prior to displacement. That is, in a single-fluid flow of fluid 2 we require the shear stress at the wall on the narrow side of the annulus to exceed the gel strength[†] of fluid 2.

(b) *Yield stress.* The yield stress of each fluid must be overcome on the narrow side of the annulus. This is achieved when the wall shear stress generated by hydrostatic pressure gradient and friction pressure gradient exceeds the yield stress of displaced fluid, that is

$$\left| \left(\frac{d\hat{P}}{d\hat{\xi}} \right)_{friction} + (\hat{\rho}_1 - \hat{\rho}_2)\hat{g} \cos \beta \right| > 2\hat{\tau}_{2,Y}/\hat{l}_n, \quad (7.1)$$

where $\hat{\cdot}$ denotes dimensional variables and \hat{l}_n is the dimensional width of the annular gap on the narrow side of the annulus.

(c) *Channelling.* The interface on the narrow side of the annulus has to move at least as fast as on the wide side to avoid channelling. This is to be achieved by either increasing the narrow-side velocity of the displaced fluid 2 or by promoting mixing and exchange of fluid around the annulus.

Versions of the first two criteria date back to the work of McLean, Manry & Whitaker (1966). Other authors also recommend that the fluids in the annulus are circulated prior to displacement, in order to condition the drilling mud (see e.g. Ravi, Beirute & Covington 1992). These criteria have been examined further in Ryan, Kellingray & Lockyear (1992), where a cementing placement simulator that assesses the quality of mud displacement is also described. In particular, the yield stress criterion has been refined to distinguish between two cases. First, when $\hat{\rho}_2 < \hat{\rho}_1$ and fluid 2 would move from the narrow side of the annulus if the vector sum of buoyancy and friction pressure forces exceed the yield limit in magnitude. Secondly, if $\hat{\rho}_2 > \hat{\rho}_1$, when fluid 2 is considered to move only in the axial direction on the narrow side and only the axial component of buoyancy and the friction pressure gradient are considered. The measure of channelling is taken to be the ratio $\hat{v}_{narrow}/\hat{v}_{average}$, where \hat{v}_{narrow} is the estimated velocity of the interface on the narrow side and $\hat{v}_{average}$ is the average velocity of fluid in the annulus. To calculate \hat{v}_{narrow} , the properties of fluid 1 are used to calculate the pressure gradient (using a slot approximation to the annular gap), and the properties of fluid 2 are used to calculate the velocity on the narrow side. This is obviously close to our approach of computing (3.34).

7.2. Effective laminar-flow design criteria

A second example of a design system, with some overlap with that of Lockyear *et al.*, is the effective laminar flow (ELF) rule system, introduced by Couturier *et al.* (1990). A similar system was also proposed earlier by Jamô^t (1974). An example of successful application is presented in Brady *et al.* (1992) and an example of usage in conjunction with rheological tools to determine (or rather *define*) optimum spacer composition is described in Theron, Bodin & Fleming (2002). A summary of these rules follows.

[†] As opposed to the yield stress, which is a dynamic property, the gel strength of the drilling mud increases when the mud is static, typically reaching an asymptote over a period of 10–60 min. It is the gel strength that must be exceeded (broken) in order for the mud to flow. Typically, this is achieved by pre-circulation. In our model, for simplicity, we assume that the mud has been circulated just prior to displacement.

(a) *Density hierarchy rule.* The displacing fluid 1 must be 10% heavier than the displaced fluid 2:

$$\hat{\rho}_1 > 1.1\hat{\rho}_2. \quad (7.2)$$

(b) *Friction hierarchy rule.* Fluid 1 must exert a friction pressure gradient that is 20% larger than that of fluid 2:

$$\left(\frac{d\hat{P}}{d\hat{\xi}}\right)_{1,friction} > 1.2\left(\frac{d\hat{P}}{d\hat{\xi}}\right)_{2,friction}. \quad (7.3)$$

The friction pressure is calculated here for a single-fluid flow in a concentric annulus of the same dimensions. This rule ensures that the displacing fluid is effectively more viscous than the displaced.

(c) *Minimum pressure gradient (MPG) rule.* Fluid 2 must be fully mobile on the narrow side of the annulus – that is, the yield stress of the displaced fluid is exceeded by the shear stress on the narrow side of the annulus:

$$\left(\frac{d\hat{P}}{d\hat{\xi}}\right)_{1,friction} > \frac{2\hat{\tau}_{2,Y}}{\hat{l}_n} + (\hat{\rho}_2 - \hat{\rho}_1)\hat{g} \cos \beta. \quad (7.4)$$

(d) *Differential velocity rule.* The displacing fluid 1 on the wide side must not go faster than fluid 2 on the narrow side – in effect, the same reasoning we used in interpreting the lubrication model above. The calculation here, however, is based on considering ‘wide’ and ‘narrow’ concentric annuli with uniform annular gap equal to that of the original annulus’ wide and narrow sides, respectively. Thereafter, the pressure gradient in fluid 1 flowing through the ‘wide’ annulus and fluid 2 flowing through the ‘narrow’ annulus, both with the average speed of the original flow, are compared. The rule is then satisfied if the pressure drop in the wide annulus is larger than the pressure drop in the narrow annulus:

$$\left(\frac{d\hat{P}}{d\hat{\xi}}\right)_{1,friction}^{wide} + \hat{\rho}_1\hat{g} \cos \beta > \left(\frac{d\hat{P}}{d\hat{\xi}}\right)_{2,friction}^{narrow} + \hat{\rho}_2\hat{g} \cos \beta. \quad (7.5)$$

Examining the rules above (in the light of our earlier results), we can see intuitively that the density and friction hierarchy rules help to avoid unsteadiness, aiding the bulk displacement. They are physically intuitive and provide quick simple criteria for fluid design, but obviously can be restrictive as they require a strict hierarchy of fluid densities and rheologies. They also do not take into account the eccentricity of the annulus, and do not consider any combination of buoyancy and viscous forces. The MPG rule provides the necessary minimum flow rate required to move the displaced fluid on the narrow side of the annulus, but does not by itself ensure the stability of displacement. On the other hand, the differential velocity rule does consider the bulk displacement stability, takes into account all of the process parameters and thus should be the criterion that is most directly comparable (in spirit) to the lubrication model described earlier.

To illustrate these rules, consider the following scenario. We fix outer and inner annular radii at 0.125 m and 0.1 m, respectively, and the flow rate at $0.01 \text{ m}^3 \text{ s}^{-1}$. For simplicity, we suppose that the displacing fluid parameters are $\hat{\rho}_1 = 1500 \text{ kg m}^{-3}$, $\hat{\tau}_{1,Y} = 10 \text{ Pa}$, $\hat{\kappa}_1 = 0.025 \text{ Pa s}$, $n_1 = 1$, and consider the effectiveness of displacing a range of fluids at different inclinations and eccentricities. The displaced fluid properties range in the $(\hat{\tau}_{2,Y}, \hat{\kappa}_2, \hat{\rho}_2)$ -space, (for ease of visualization, we also fix $n_2 = 1$). The individual

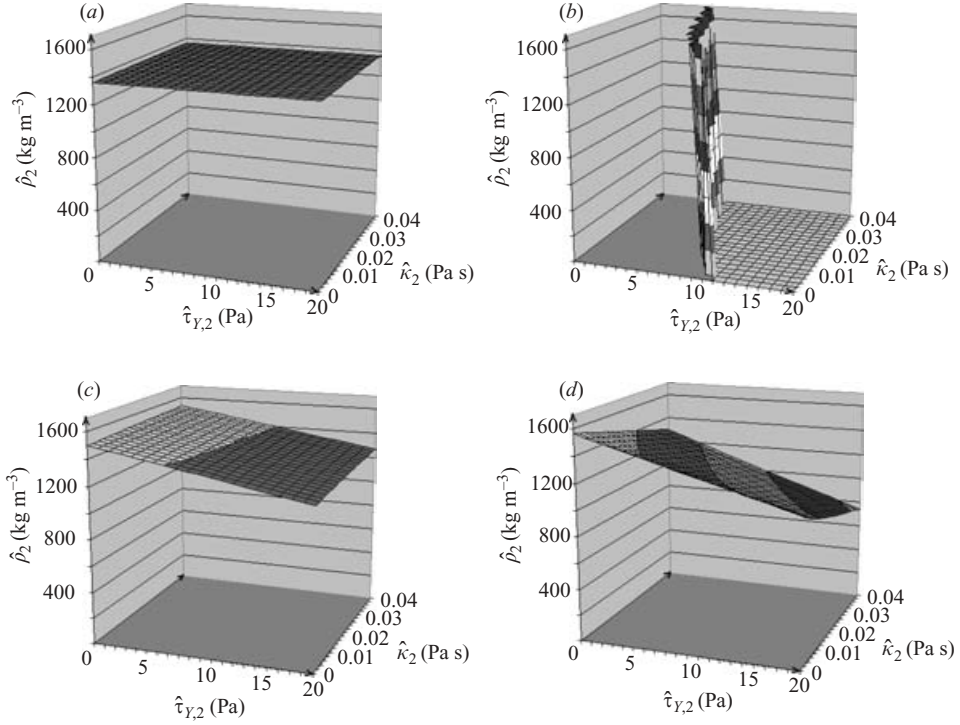


FIGURE 17. The individual ELF rules illustrated. (a) Density hierarchy; (b) friction hierarchy; (c) minimum pressure gradient; (d) differential velocity. In each case, the rule is satisfied to the left and underneath the surface illustrated. Displacing fluid parameters: $\hat{\rho}_1 = 1500 \text{ kg m}^{-3}$, $\hat{\tau}_{1,Y} = 10 \text{ Pa}$, $\hat{\kappa}_1 = 0.025 \text{ Pa s}$, $n_1 = 1$; outer and inner annular radii are 0.125 m and 0.1 m , respectively, flow rate at $0.01 \text{ m}^3 \text{ s}^{-1}$, $n_2 = 1$, $\beta = 0$, $e = 0.6$.

rules are shown in figure 17, with $\beta = 0$, $e = 0.6$. To satisfy each rule, the parameters ($\hat{\tau}_{2,Y}$, $\hat{\kappa}_2$, $\hat{\rho}_2$) must be below the surface illustrated. As the rules are combined together, we see that in different parameter ranges, different constraints are more or less active. For example, for near-vertical wells with small to moderate eccentricity, only the density and friction hierarchies come into play, as the most conservative. These appear as a horizontal roof for the density hierarchy and a vertical wall for the friction hierarchy. For higher inclinations and eccentricities, the differential velocity criterion starts to appear as a slanted roof. The MPG criterion is rarely active, except in highly eccentric wells.

We make three comparisons between the combined set of ELF rules and the lubrication model prediction of a steady displacement. The first two comparisons (figures 18 and 19) are in vertical wells with eccentricities $e = 0.2$ and $e = 0.6$, respectively. In figure 20, we show a comparison at high inclination, ($\beta = 60^\circ$), and high eccentricity.

In each figure, the lubrication model makes a prediction of a steady displacement for parameters at which the ELF rule-based system would not predict a good displacement, i.e. the ELF rules predictions are generally more conservative. The degree of conservatism can be high, especially when the frictional pressure criterion is not satisfied. When this criterion is satisfied, the density hierarchy appears to be conservative by somewhere in the range of 3–10%. For inclined eccentric displacements (figure 20),

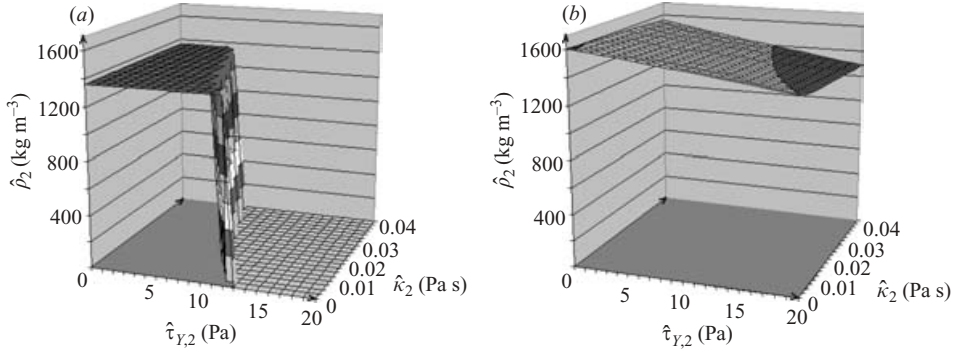


FIGURE 18. Comparison of (a) the ELF rules design criteria with (b) the lubrication criteria at $e=0.2$, $\beta=0$.

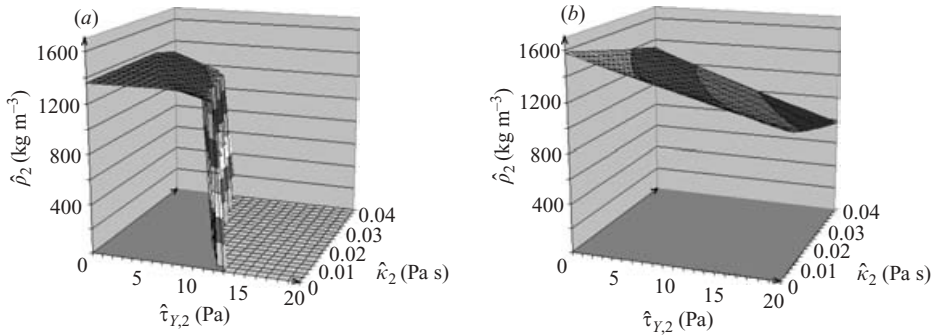


FIGURE 19. Comparison of (a) the ELF rules design criteria with the (b) lubrication criteria at $e=0.6$, $\beta=0$.

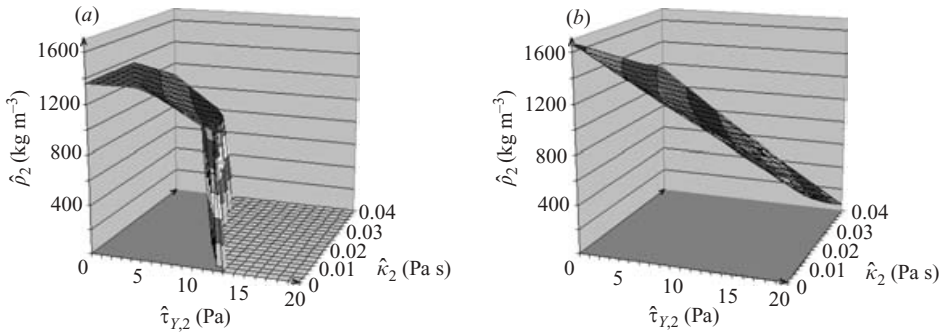


FIGURE 20. Comparison of (a) the ELF rules design criteria with (b) the lubrication criteria at $e=0.6$, $\beta=60^\circ$.

we see that the differential velocity criterion becomes an increasingly active constraint and that this constraint surface parallels that of the lubrication model. This is not surprising, since the lubrication model is also a differential velocity criterion, although based on a more rational computation of the interface velocity.

Also in other parameter ranges computed, we have always found the ELF rule-based system to be conservative by comparison with the lubrication modelling approach. The examples we have presented are indeed quite favourable to the ELF system.

This is because in these displacements, the density hierarchy is very active, taking the place mostly of the differential velocity criterion. Sources of conservatism are straightforward to identify. First, the ELF system seeks to satisfy all criteria individually, whereas the lubrication approach, being an actual computation of interface velocity, allows compensation between competing effects. Secondly, the computation of the frictional pressure hierarchy does not include any effect of eccentricity. Thirdly, the differential velocity criterion does not compute velocities accurately. However, although conservative, the ELF system is physically sensible in its predictions.

8. Summary of results

The main thrust of the paper has been to analyse the Hele-Shaw displacement model of Bittleston *et al.* (2002), for the case of a two-fluid displacement along a uniform inclined eccentric annulus. In particular, we have focused on the derivation of simple expressions that define parameter regimes where steady/unsteady and locally stable/unstable displacements occur. We may summarize the key results as follows.

(a) In §3.2, we have derived conditions under which the displacement front is likely to be steady (i.e. a travelling-wave solution) or unsteady. In the latter case, we may also classify whether or not the displaced fluid (drilling mud in the industrial application) will remain stuck on the narrow side of the annulus. What differentiates our results from others (e.g. those currently used in the petroleum industry, see §7) is that ours are derived from the Navier–Stokes equations using accepted and well-defined scaling arguments, instead of by using *ad hoc* assumptions regarding hydraulic flows.

(b) In §3.3 and §3.4, we derive simple sufficient conditions for an unsteady displacement (3.32), and conditions for local instability of the interface on the wide and narrow sides of the annulus, (3.33) and (3.34). These conditions are evaluated by quadrature from the eight dimensionless parameters that characterize the displacement.

(c) For small eccentricities ($e \ll 1$), we have been able to derive explicit analytical expressions for our stability criteria (3.32)–(3.34), in the case that the fluids are either Newtonian (§4.1) or power law (§4.2). We have also been able to give analytical expressions that predict the wide–narrow side velocity differential. This is the speed at which an unsteady interface would propagate ahead on the wide side.

(d) For small eccentricities and ‘moderate’ buoyancy parameter† we have demonstrated that if (3.33) and (3.34) are satisfied, then (3.32) will also be satisfied, i.e. local instability of the wide and narrow side will imply that the interface is unsteady, but not vice versa. The criteria for unsteady and unstable interfaces coincide at $e = 0$. For larger e and $|b|$ we have no explicit analytical result, but there is nothing contradictory in the results we have computed.

(e) For $e > 0$, there is a natural tendency towards an unsteady displacement front, which is most easily explained as a dispersion phenomenon (i.e. for a single fluid displacing itself). Dispersive effects can be countered by either increasing the effective viscosity of the displacing fluid or reducing b . A number of computed examples in §§5 and 6 have illustrated this.

(f) The transition from an unsteady displacement to a steady displacement as model parameters are changed appears to be characterized by the development of shocks on the wide and narrow sides of the annulus, and their eventual coalescence. Thus, a steady state in terms of our lubrication model corresponds to a single shock discontinuity filling the annulus, i.e. the steady state has no shape.

† ‘Moderate’ meaning the modified pressure gradients in both fluids have the same sign.

(g) In the case of no buoyancy, the model depends upon six dimensionless rheological parameters and the eccentricity. Other than for small eccentricity, analytical results are not possible. In general, displacement is enhanced (meaning that the wide–narrow side velocity differential is reduced) when the effective viscosity of the displacing fluid is increased or when the eccentricity is reduced.

(h) In general, $b < 0$ will aid displacement. When $b \neq 0$ and $|b|$ is large, the situation can become quite complicated and we have not fully analysed this case.

(i) Finally, in §7 we have shown that our results compare favourably with those from systems of design rules currently used in industry, in that they predict similar trends, but are less conservative.

Parts of this work have been carried out at the University of British Columbia, supported financially by Schlumberger and the NSERC through CRD project 245434, as well as by the Pacific Institute for the Mathematical Sciences. This support is gratefully acknowledged. We acknowledge the permission of the management of Schlumberger for allowing us to publish parts of this work. We thank Dr Dominique Guillot for his valuable insights. We would like to thank the referees for their helpful comments on the first version of our paper.

REFERENCES

- ALEXANDROU, A. N. & ENTOV, V. 2000 On the steady-state advancement of fingers and bubbles in a Hele-Shaw cell filled by a non-Newtonian fluid. *Eur. J. Appl. Maths* **8**, 73–87. Q2
- ALLOUCHE, M., FRIGAARD, I. A. & SONA, G. 2000 Static wall layers in the displacement of two visco-plastic fluids in a plane channel. *J. Fluid Mech.* **424**, 243–277.
- BALMFORTH, N. J. & CRASTER, R. V. 1999 A consistent thin-layer theory for Bingham plastics. *J. Non-Newtonian Fluid Mech.* **84**, 65–81.
- BARENBLATT, G. I., ENTOV, V. M. & RYZHIK, V. M. 1990 *Theory of Fluid Flows Through Natural Rocks. Theory and Applications of Transport in Porous Media*, vol. 3, pp. 44–51, 187–229. Kluwer.
- BITTLESTON, S. H., FERGUSON, J. & FRIGAARD, I. A. 2002 Mud removal and cement placement during primary cementing of an oil well; laminar non-Newtonian displacements in an eccentric Hele-Shaw cell. *J. Engng Maths* **43**, 229–253.
- BRADY, S. D., DRECO, P. P., BAKER, K. C. & GUILLOT, D. J. 1992 Recent technological advances help solve cement placement problems in the Gulf of Mexico. *Soc. Petrol. Engrs Paper IADC/SDPE 23927*.
- COCKBURN, B. & SHU, C.-W. 1994 Nonlinearly stable compact schemes for shock calculations. *SIAM J. Numer. Anal.* **31**, 607–627.
- COUSSOT, P. 1999 Saffman–Taylor instability in yield-stress fluids. *J. Fluid Mech.* **380**, 363–376.
- COUTURIER, M., GUILLOT, D. J., HENDRIKS, H. & CALLET, F. 1990 Design rules and associated spacer properties for optimal mud removal in eccentric annuli. *Soc. Petrol. Engrs Paper SPE 21594*.
- FENIE, H. & FRIGAARD, I. A. 1999 Transient fluid motions in a simplified model for oilfield plug cementing. *Math. Comput. Mod.* **30**, 71–91.
- GOLDSTEIN, R. V. & ENTOV, V. M. 1989 *Qualitative Methods in Continuum Mechanics*. Longman Wiley. 279 pp.
- JAMÔT, A. 1974 Déplacement de la boue par le latier de ciment dans l'espace annulaire tubage-paroi d'un puits. *Rev. Assoc. Franc. Tech. Petr.* **224**, 27–37.
- LINDNER A. 2000 L'instabilité de Saffman–Taylor dans les fluides complexes: relation entre les propriétés rhéologiques et la formations de motifs. These de l'Universite Paris VI (PhD thesis), Paris, France.
- LINDNER, A., COUSSOT, P. & BONN, D. 2000 Viscous fingering in a yield stress fluid. *Phys. Rev. Lett.* **85**, 314.

- LIPSCOMB, G. G. & DENN, M. M. 1984 Flow of Bingham fluids in complex geometries. *J. Non-Newtonian Fluid Mech.* **14**, 337–346.
- LOCKYEAR, C. F. & HIBBERT, A. P. 1989 Integrated primary cementing study defines key factors for field success. *J. Petrol. Technol.* December, 1320–1325.
- LOCKYEAR, C. F., RYAN, D. F. & GUNNINGHAM, M. M. 1989 Cement channeling: how to predict and prevent. *Soc. Petrol. Engrs Paper SPE* 19865.
- MCLEAN, R. H., MANRY, C. W. & WHITAKER, W. W. 1966 Displacement mechanics in primary cementing. *Soc. Petrol. Engrs Paper SPE* 1488.
- MUSKAT, M. 1937 *The Flow of Homogeneous Fluids Through Porous Media*. McGraw-Hill.
- NELSON, E. B. 1990 *Well Cementing*. Schlumberger Educational Services.
- PASCAL, H. 1984a Rheological behaviour effect of non-Newtonian fluids on dynamic of moving interface in porous media. *Intl J. Engng Sci.* **22**, 227–241.
- PASCAL, H. 1984b Dynamics of moving interface in porous media for power law fluids with a yield stress. *Intl J. Engng Sci.* **22**, 577–590.
- PASCAL, H. 1986 A theoretical analysis of stability of a moving interface in a porous medium for Bingham displacing fluids and its application in oil displacement mechanism. *Can. J. Chem. Engng* **64**, 375–379.
- PELIPENKO, S. & FRIGAARD, I. A. 2004a On steady state displacements in primary cementing of an oil well. *J. Engng Maths* **48**, 1–26.
- PELIPENKO, S. & FRIGAARD, I. A. 2004b Two-dimensional computational simulation of eccentric annular cementing displacements. *IMA J. Appl. Maths* **64**.
- RAVI, K. M., BEIRUTE, R. M. & COVINGTON R. L. 1992 Erodability of partially dehydrated gelled drilling fluid and filter cake. *Soc. Petrol. Engrs Paper SPE* 24571.
- RYAN, D. F., KELLINGRAY, D. S. & LOCKYEAR C. F. 1992 Improved cement placement on North sea wells using a cement placement simulator. *Soc. Petrol. Engrs Paper SPE* 24977.
- SZABO, P. & HASSAGER, O. 1992 Flow of viscoplastic fluids in eccentric annular geometries. *J. Non-Newtonian Fluid Mech.* **45**, 149–169.
- THERON, B. E., BODIN, D. & FLEMING, J. 2002 Optimization of spacer rheology using neural network technology. *Soc. Petrol. Engrs Paper SPE* 74498.
- WALTON, I. C. & BITTLESTON, S. H. 1991 The axial flow of a bingham plastic in a narrow eccentric annulus. *J. Fluid Mech.* **222**, 39–60.